MET O 11 TECHNICAL NOTE. NO. 177

Three Dimensional Vortex Methods for Turbulence Simulation

Part 1. Investigation of Singular Solutions to Euler's Equations

by

S. P. Ballard

Meteorological Office (Met O 11)

London Road

Bracknell

Berkshire

United Kingdom

1. Introduction

Recent work by Chorin (1981, 1982) using a three dimensional vortex method, suggests that, if incompressible, inviscid flow can be described by Euler's equations, the vorticity becomes infinite in finite time for all but special initial data. Work by Morf, Orszag and Frisch (1980) and Brachet et al (1983) also indicates that there may be a singularity in finite time. This has important implications for any models using the inviscid, incompressible equations of motion with sub-grid scale parametrizations as the problem may be ill-determined and the solution may not necessarily converge as the mesh size is reduced, see Cullen (1983). Results may be very dependent on the form of artificial viscosity that is used. This is becoming increasingly important in meteorology as we seek to resolve motions of ever decreasing scales.

A further result of Chorin's work is that the vorticity stretches unevenly and that the highly stretched vorticity collects itself into a body with shrinking volumne. He calculates that the L_2 support of the vorticity shrinks to an object of Hausdorff dimension of approximately 2.5 as predicted by Mandelbrot (1972, 1974). This is not discussed here but will be the subject of future investigations, as the intermittency of the turbulence implied by a Hausdorff dimension between 2 and 3 will again have implications in atmospheric modelling, particularly in the form of closures used for modelling three dimensional turbulence.

It is important, therefore, to verify the work of Chorin on the inviscid problem and then, by adding viscosity, attempt to simulate three dimensional turbulence in order to provide a means of checking turbulence parametrizations currently used in finite difference methods. The high resolution of vortex methods in the regions of fluid containing vorticity

allow smaller scales of motion to be resolved than equivalent conventional grid point methods. The extension to viscous flow will be a subject of future work.

In general, vortex methods approximate the vorticity of a fluid by collections of 'vortex elements' such as point vortices or sheets in 2 dimensions and by line vortices, tiles or line segments in 3 dimensions, see the review by Leonard (1980), and then follow their movements in order to study the behaviour of the flow. The high velocities induced in the flow by these singular distributions of vorticity are suppressed by considering the vortex elements to have a finite core, or associated non-singular distribution of vorticity, allowing stable solutions of the equations of motion by distorting the close interaction of the elements. Mathematical proofs of the convergence of vortex methods, see Hald (1979) and Beale and Majda (1982a), basically use the finite core of the elements as a means of providing stability and avoiding infinite induced velocities, once sufficient resolution of the vorticity field has been obtained. However it is also possible to consider the smoothed equations as exact solutions for the vorticity field composed of elements with small support, such that the vorticity vanishes outside the core. A further viewpoint is to consider the vortex method as a means of approximating a velocity field, rather than the vorticity field, such that the distribution of vortex elements is found such that the best approximation to the velocity is made rather than the vorticity. Hence it may be possible to consider a general flow containing widely distributed vorticity to be approximated by that due to vortex elements concentrated only in the regions of high vorticity or that simply the evolution of the general flow described by the initial vortex elements is being studied.

When the evolution of the flow associated with a region of vorticity whose support is covered by single elements, in the plane perpendicular to the direction of the vorticity, is considered it is not obvious what situation is being modelled. Chorin (1982) follows the evolution of the configuration of single vortex filaments with an associated core of constant radius, thus it can be argued that he is either modelling the case of single line vortices, vortex tubes with vanishingly small cross-sections, where the core size just produces stability and removes the singularity, or that of a vorticity field composed of elements with small support, given by the core size, or an approximation to a flow containing more widepsread vorticity. It is important to ensure that the initial data is not singular when considering the finite time 'blow-up' of the Euler equations and to consider the implications of the use of a given core size, a matter of controversy in the field of vortex methods. The work discussed in this technical note attempts to address this problem and results indicate that the core size represents the size of the cross-section of a vortex tube but further studies increasing the resolution in the cross-section are required in order to verify that conclusion.

Our attempts to reproduce the evolution of a turbulent vortex, described by Chorin (1982), found that the evolution was dependent on the time integration scheme and the size of the time steps used. However all runs eventually produced a rapid increase in 'vorticity' as measured by the L_1 and L_2 norms. To overcome this apparent lack of consistency in the results and to use smoother initial data, particularly without the problem of the initial representation of curved vortex filaments, Chorin's method has been extended to consider the evolution of a periodic lattice of straight vortex filaments. This has also enabled direct comparison with

the implementation of another three dimensional method described by Beale and Majda (1982 a) and b)) that they proved to be stable and convergent for a smooth, initial velocity field with initial vorticity of bounded support.

One important result of this work is the identification of the possible role of the mechanism of pairing of opposite signed vorticity in the rapid production of vorticity whilst conserving energy. This has been noted in previous work, for example Chorin (1982) as a means of conserving energy but not as a way of amplifying the increase in vorticity. It also suggests a method of including viscosity in the method by removing portions of filaments where pairing has occurred. This is supported by laboratory experiments, see Leonard (1980) for references, where filament loops in proximity may, depending on their relative orientation, attract each other to the extent that their vorticity fields are cancelled significantly where they overlap.

This technical note sets out the theory behind vortex methods, as well as the details of Chorin's and Beale and Majda's methods, in section 2. Section 3 deals with the numerical techniques employed and the diagnostics produced for each of the methods in the case of a periodic lattice of filaments. The results of the integrations are presented in section 4 and the conclusions in section 5.

2. Vortex Methods for Flow Simulation

2.1 Theoretical Background

The Euler Equations for three dimensional, incompressible, inviscid flow are

$$\frac{\partial \vec{\omega}}{\partial t} + (\vec{u}\cdot\nabla)\vec{\omega} = (\vec{\omega}\cdot\nabla)\vec{u} \qquad (1)$$

$$\vec{\omega} = \nabla \times \vec{u} \tag{2}$$

$$\nabla \cdot \vec{u} = 0 \tag{3}$$

where $\vec{\omega}$ is the vorticity, $\vec{u}$ the velocity and ∇ the differentiation vector.

The combination of equations (2) and (3) gives the Poisson Equation

$$\nabla^2 \vec{u} = -\nabla \times \vec{\omega} \tag{4}$$

If $\vec{u} \cdot \vec{n} \Big|_{\text{Surface}} = 0$ ie the normal components of velocity on the boundaries are zero the solution to (4) may be written as the Biot-Savart integral

$$\vec{u}(\vec{x},t) = -\frac{1}{4\pi} \int \frac{(\vec{x}-\vec{x}') \times \vec{\omega}(\vec{x}',t)\, d\vec{x}'}{|\vec{x}-\vec{x}'|^3}$$

Hence the fluid velocity is uniquely determined kinematically from the vorticity field. Since from the theorems of Helmholtz and Kelvin we know that the inviscid motion of the vorticity is given by the local fluid velocity we can consider inviscid fluid dynamics in terms of parcels of vorticity which induce motion on each other as an alternative to the pressure-velocity description. This is particularly useful when the flow is characterized by regions of concentrated vorticity in otherwise irrotational fluid, such as can occur in incompressible flows at high Reynolds numbers. Then the computational points will be concentrated in the regions of interest in the flow.

Simple motions illustrating the mutual induction processes are a vortex ring propelling itself along its axis and a pair of aircraft trailing vortices inducing downward motion upon each other. Flows of this type can be simulated by discretizing the vorticity containing regions and tracking the discretization in a Lagrangian reference frame.

2.2 Chorin's Method

Chorin considers the solution of Euler's Equations in a unit cube box with periodic boundary conditions. He supposes that the initial data can be approximated by M vortex tubes or filaments of small but finite cross-section. The circulation of the ith tube is Γ_i,

$$\Gamma_i = \int_{\text{cross-section}} \vec{\omega} \cdot d\vec{A} \quad = \text{constant of motion}$$

Then, if $\vec{x}(t)$ is the position vector of a point moving with the fluid, the velocity $\vec{u}(\vec{x},t)$ induced by the filaments at $\vec{x}(t)$ can be approximated by the Biot-Savart Law

$$\vec{u}(\vec{x},t) = -\frac{1}{4\pi} \sum_{i=1}^{M} \Gamma_i \int_{i\text{th filament}} \frac{\vec{a} \times d\vec{s}}{|\vec{a}|^3}$$

where $\vec{s} = \vec{s}(\vec{x}',t)$ is the unit tangent to the ith filament at $\vec{x}'$

ds is the element of arc length along the direction $\vec{s}$

$$d\vec{s} = \vec{s}\, ds$$

$$\vec{a} = \vec{x}(t) - \vec{x}'(t)$$

Since the expression for the velocity is singular when $\vec{x}$ (t) lies on a filament the velocity is then given approximately by

$$\vec{u}(\vec{x},t) = -\frac{1}{4\pi}\sum_{i=1}^{M}\Gamma_i \int_{i\text{th filament}} \frac{\vec{a}\times d\vec{s}}{\psi(a)}$$

where

$$\psi(a) = \begin{cases} |\vec{a}|^3 & \text{if } |\vec{a}| \geq R_{min} \\ |\vec{a}|\, R_{min}^2 & \text{if } |\vec{a}| < R_{min} \end{cases}$$

The function ψ (a) is introduced to take account of the finite cross-section of the filaments to avoid the infinite velocity induced by close-neighbour interaction on infinitely thin filaments.

The motion of points are given by

$$\frac{d\vec{x}(t)}{dt} = \vec{u}(\vec{x},t)$$

The vortex filaments are further approximated by N_i vortex segments of length ΔS_j^i , $i=1,M$, $j=1,N_i$ and circulation Γ_i , see figure 2.1 The motions of the centres of the end points of the segments are followed, so that the vortex stretching is represented by the increase in separation of adjacent nodes, ie the increase in length of the vortex segments.

The velocity of the nodes (endpoints) is given by

$$\vec{u}(\vec{x}_l^n) = -\frac{1}{4\pi}\sum_{i=1}^{M}\Gamma_i \sum_{j=1}^{N_i} \frac{\vec{a}_{jl}^{in}\times\Delta\vec{s}_j^i}{\psi(\vec{a}_{jl}^{in})}$$

where $n = 1,M \qquad l = 1,N_n$

$$\Delta\vec{s}_j^i = \vec{x}_{j'}^i - \vec{x}_j^i \quad , \quad j' = (j+1) \bmod (N_i)$$

$$\vec{a}_{jl}^{in} = \frac{1}{2}(\vec{x}_{j'}^i + \vec{x}_j^i) - \vec{x}_l^n$$

The lengths of the segments $\Delta \vec{s}_j^{\,i}$ are limited to some value ℓ. Once this value is exceeded the segments are split at their midpoints such that if

$$|\Delta \vec{s}_j^{\,i}| > \ell$$

$$N_i \Rightarrow N_i' = N_i + 1$$

$$\Delta \vec{s}_j^{\,i} = \Delta \vec{s}_k^{\,i} + \Delta \vec{s}_{k'}^{\,i}$$

where $k = j$, $k' = (j+1) \bmod (N_i + 1)$

$$\Delta \vec{s}_k^{\,i} = \frac{1}{2}\left(\vec{x}_{j'}^{\,i} + \vec{x}_j^{\,i}\right) - \vec{x}_j^{\,i} \quad , \quad j' = (j+1) \bmod (N_i)$$

$$\Delta \vec{s}_{k'}^{\,i} = \vec{x}_{j'}^{\,i} - \frac{1}{2}\left(\vec{x}_{j'}^{\,i} + \vec{x}_j^{\,i}\right)$$

Therefore the number of points followed increases as the length of the filaments, and hence the vorticity, increases.

Since there are an infinite number of image vortex filaments to be considered in a periodic domain, the number of images considered must be limited. This is done by applying a maximum cut-off value, Rmax, to $|\vec{a}_{jl}^{\,in}|$ so that segments of separation greater than Rmax from a given node $\vec{x}_l^{\,n}$ are not included in the velocity calculation. Hence if Rmax < 0.5 only one 'nearest' image needs to be considered.

ie. $$\frac{1}{\psi(\vec{a}_{jl}^{\,in})} = 0 \quad \text{if} \quad |\vec{a}_{jl}^{\,in}| > \text{Rmax}$$

The motion of the nodes is given by

$$\frac{d\vec{x}_l^{\,n}(t)}{dt} = \vec{u}\left(\vec{x}_l^{\,n}(t)\right)$$

Obviously the solutions may depend on the three parameters, Rmin, Rmax and ℓ as well as the time integration scheme and the dependence on these must be ascertained. Trial integrations in which these

parameters are varied are discussed in Section 4. The dependence on Rmax and ℓ is found to be weak, increasing Rmax and decreasing ℓ both increase the resolution in the method and improve the accuracy of the solution. However the parameter Rmin and the function $\eta(\alpha)$ affect the form of the solution as the variable Rmin appears to represent the radius of cross-section of a vortex, in the case of one filament per vortex, and the function $\eta(\alpha)$ is linked to the vorticity distribution within the core of the vortex.

2.3 Beale and Majda's Method

In the algorithms described in Beale and Majda (1982 a) and b)) the velocity is updated crudely similarly to Chorin's method. However the vortex stretching is now incorporated via a Lagrangian update.

For position $\vec{x}(t) = (x_1, x_2, x_3)$

fluid velocity $\vec{u}(\vec{x}(t)) = (u_1, u_2, u_3)$

and vorticity $\vec{\omega}(\vec{x}(t)) = (\omega_1, \omega_2, \omega_3)$

the trajectory $\vec{x}_\alpha(t)$ of a fluid particle starting at time zero at the position $\vec{x}_\alpha(0) = \vec{\alpha} = (\alpha_1, \alpha_2, \alpha_3)$ is again determined by the equation

$$\frac{d\vec{x}_\alpha(t)}{dt} = \vec{u}(\vec{x}_\alpha(t)) \quad , \quad \vec{x}_\alpha(0) = \vec{\alpha}$$

The expression for the velocity, the Biot-Savart law is used in the form

$$\vec{u}(\vec{x}_\alpha(t)) = \int_{R^3} K(\vec{x}_\alpha - \vec{x}') \times \vec{\omega}(\vec{x}'(t))\, d\vec{x}'$$

where K is the matrix value kernel.

$$K(\vec{x}) = -\frac{1}{4\pi} \frac{\vec{x}}{|\vec{x}|^3}$$

The stretching of vorticity can be described by the vorticity equation

$$\frac{\partial \vec{\omega}}{\partial t} + \vec{u} \cdot \nabla \vec{\omega} = \vec{\omega} \cdot \nabla \vec{u}$$

$$\text{or} \quad \frac{d \vec{\omega}}{dt} = \vec{\omega} \cdot \nabla \vec{u}$$

This can be expressed in a Lagrangian formula

$$\frac{d \omega (\vec{x}_\alpha(t))}{dt} = \vec{\omega} (\vec{\alpha}, 0) \cdot \nabla_\alpha \vec{u} (\vec{x}_\alpha(t))$$

see Milne-Thomson (1968) or Holt (1982), involving the gradients of velocity at time t with respect ot the initial positions of the points $\vec{x}_\alpha(t)$ where $\nabla_\alpha \vec{u} (\vec{x}_\alpha(t))$ is the 3 x 3 Jacobian matrix

$$\frac{\partial u_i (\vec{x}_\alpha(t))}{\partial \alpha_j} \qquad 1 \leq i, j \leq 3$$

and $\vec{\omega} (\vec{\alpha}, 0) = \vec{\omega} (x_\alpha(0))$ is the initial vorticity.

The initial vorticity fields are discretized onto a three dimensional uniform grid of grid step h. Values of position, velocity and vorticity are held on this grid, the grid data points moving with the fluid but the velocity derivatives being calculated with respect to their initial positions, thus minimizing errors due to errors in evolving quantities. There are thus two coupled nonlinear ordinary differential equations

$$\frac{d \vec{x}_i (t)}{dt} = u_i^h (t) \qquad \vec{x}_i (0) = (lh, mh, nh)$$

$$\frac{d \vec{\omega}_i (t)}{dt} = \nabla_\alpha^h u_i^h (t) \cdot \vec{\omega}_i (0) \qquad \vec{\omega}_i (0) = \vec{\omega} (\vec{x}_i 0))$$

and since for $\vec{\omega}_i(0) = 0$, $\dfrac{d\vec{\omega}_i(t)}{dt} = 0$

data need only be held on a set of points slightly larger than the set of points falling in the support of the initial vorticity field.

The kernel K is replaced by a smoothed kernel K_δ where

$$K_\delta(\vec{x}) = \int K(\vec{x}-\vec{x}')\chi_\delta(\vec{x}')\,d\vec{x}'$$

and $$\chi_\delta(\vec{x}') = \delta^{-3}\chi\left(\frac{\vec{x}'}{\delta}\right)$$

χ being a similar cut-off function satisfying $\int \chi\, d\vec{x}' = 1$ and other stability and accuracy conditions, see Beale and Majda 1982a) and 1983. Thus $u_i^h(t) = \sum_j K_\delta(\vec{x}_i(t) - \vec{x}_j(t)) \times \omega_j(t) h^3$

3. Comparison of the Two Vortex Methods for Simple Initial Data

3.1 Form of Initial Data

Chorin's (1982) data contained sharp discontinuities in the gradient of the space curve describing the filament, see figure 3.1, this has aroused concern about the nature of the initial data since it is not clear whether the vortex segments are an approximation to a smooth vorticity distribution, such as a curved filament, or one containing sharp corners. Also his time integration scheme, Euler's

method, was very crude and started with a long initial time step. When the same initial conditions were used with a variety of time-integration schemes the vorticity was stable for varying lengths of time. However the evolution of the vorticity for all cases showed the same general pattern, the L_1 and L_2 norms remaining nearly constant for a period of time and then rapidly increasing.

Direct comparison of the Beale and Majda method and Chorin's method, without the problem of the initial representation of curved vortex filaments is possible by considering the evolution of a periodic lattice of straight vortex filaments. Each unit cube contains two filaments crossing at right angles, separated by 0.1 units, see figures 3.2, 4.1a) and 4.1b). One filament has vorticity parallel to the x axis and the other parallel to the y axis, each having unit circulation and an assumed radius of 0.025 units.

3.2 Implementation of Chorin's Method for Periodic Lattice

3.2 a) Numerical Technique

A maximum cut-off of Rmax = 0.495 was used for most of the integrations and a limiting segment length of $\ell = 0.05$.

A slightly different function $\psi(a)$ was used to that described earlier to allow direct comparison with the Beale and Majda method.

$$\psi(a) = |\vec{a}|^3 \qquad R_{min} < |\vec{a}| \leq R_{max}$$
$$\psi(a) = R_{min}^3 \qquad |\vec{a}| \leq R_{min}$$
$$\psi(a) = \infty \qquad |\vec{a}| > R_{max}$$

with Rmin = 0.05

A fourth-order Runge-Kutta time integration scheme was used for most integrations with a time step of 0.001s. An arbitrary test for stability was used as in Chorin (1982) comparing the product of the

time step, dt, and umax, the maximum velocity of a node calculated at each time step, with a distance F = 0.03, chosen to be shorter than the maximum segment length. The time step was reduced if dtxumax was larger than F.

However in most runs using Chorin's method this limit was not exceeded and a constant time step of 0.001 s was used. It may be that a more accurate stability criteria could be used but it is not known to the author.

The final form of the program utilized the initial symmetry of the data in order to limit the number of calculations per time step and to preserve the symmetry at later times. Runs without this simplification began to lose symmetry due to rounding errors and this was particularly evident after about 300 time steps. Most calculations were performed in single precision on an IBM 3081 and the positions and velocities of the nodes stored in single precision. Double precision was used for large sums such as involved in the velocity calculations and L_1 and L_2 norms of vorticity.

The initial data contains symmetry since the initial position vectors of the filaments, $\vec{X}_A$ and $\vec{X}_B$ are

$$\vec{X}_A = (0.0, x_2, -0.05) \qquad -0.5 \leq x_2 \leq 0.5$$

$$\vec{X}_B = (x_1, 0.0, 0.05) \qquad -0.5 \leq x_1 \leq 0.5$$

The flow is considered inside the unit cube

$-0.5 \leq x_i < 0.5$ $\quad i = 1, 2, 3$ with periodic boundary conditions. At all times the flow at $z < 0$ can be obtained from that calculated at $z > 0$

Since if $\vec{u}(x_1, x_2, x_3) = (u_1, u_2, u_3)$

$\vec{u}(x_2, x_1, -x_3) = (u_2, u_1, -u_3)$

Thus the velocities and positions of only one filament need to be calculated and they are then applied to the second filament.

The motions of the node points are given as the finite difference solution to the equations

$$\frac{d\vec{x}(t)}{dt} = \vec{u}(t)$$

The lengths of the segments dl are calculated after every time step and the segments are split at their midpoints if $dl > \ell$ producing more node points to be followed at subsequent time steps.

Initially integrations were run starting with the two filaments each split into N equal length segments, typically of length $dl = \ell = 0.05$. However, after running for sufficient time that the filaments had stretched substantially, and trying different values of dl such as $\ell/2$ and $\ell/4$ it was obvious that better resolution, with fewer points, could be obtained by only decreasing the initial values of dl in the regions where rapid stretching occurred. Hence initial segments of unequal lengths were used varying from $dl = \ell = 0.05$ to $dl = \ell/128$.

The standard integration, referred to in Section 4, thus has unequal length initial segments, as described above, Rmin = 0.05, Rmax = 0.495, $\ell = 0.05$, time step dt = 0.001 and 4th order Runge-Kutta time integration scheme. Tests were carried out using equal length initial segments, Rmax = 0.995, different time integration schemes and different forms of the function $\eta(a)$. The effect of increasing Rmax, in order to include more points in the velocity calculations had little

effect on the solution, as did the equal length initial segments. When Rmax was increased, with the other variables unchanged from the standard case, so that the accuracy of the calculations should increase, the only effect on the results was to produce a slightly less rapid increase in the L_1 and L_2 norms of vorticity. The effect of equal length initial segments, with lower resolution, and the other variables unchanged was to produce a slightly more rapid increase in the L_1 and L_2 norms. Changes to the time integration schemes and the function $\gamma_{\psi(a)}$ had far greater effects as discussed in section 4.

3.2 b) Diagnostics - Stretching

The amount of stretching is followed as in Chorin (1981, 1982) using a tag Q where, initially, for N segments per unit length along a filament and hence N+1 node points

$$Q_i = \frac{1}{Vol_i} \qquad i = 1, N+1$$

where Vol_i = volume of the ith segment

$$= \pi r^2 \, dl_i$$

where r = the initial radius of the filament = 0.025.

dl_i = length of the ith segment

The volume, and hence tag of the initial segments, is constant but if a segment is split at its midpoint the tag must be doubled, since the volumes of the half segment are equal, and the same value assigned to each half-segment. If one segmenet is split there will then be N+2 node points, N+1 segments and N+2 tags Q_i per filament. Hence the value of the tag for a segment is a measure of the amount of stretching it has undergone.

3.2 c) Diagnostics - Scale Collapse.

As a segmenet stretches its radius must shrink in order to conserve volume. Moore and Saffman (1972) suggest that the radius will remain independent of position along the filament by arguing that internal waves within the filament would act to smooth out any variations along the length of the filament. However, if as in Chorin (1981, 1982) the radius variation is not smoothed along the filament, its minimum value at a given time may give an indication of the scale collapse of the motion. This needs to be verified by use of fourier analysis of the induced velocity field in a unit cube of the fluid.

$$r_i(t) = \sqrt{\frac{1}{Q_i \pi \, dl_i}} = \text{radius of the ith segment}$$

where dl_i = length of segment at time t

Q_i = value of tag for ith segment at time t.

3.2 d) Diagnostics - L_1 and L_2 Norms of Vorticity

The L_1 norm of vorticity is defined as the integral of the vorticity norm over volume

$$L_1(\omega) = \int |\vec{\omega}| \, dV$$

However the circulation Γ is given by

$$\Gamma = \int \vec{\omega} \cdot n \, dA$$

In this case $\Gamma = 1$ for each filament, since $\vec{\omega}$ is perpendicular to the cross-section and parallel to the length of the segment

$$\Gamma = \int |\vec{\omega}| \, dA = 1$$

and hence the L_1 norm is

$$L_1(\omega) = \int |\vec{\omega}| \, dA \, dl = \sum_{i=1}^{M} \sum_{j=1}^{N} dl_{ij}$$

That is the L_1 norm of vorticity is given by the total lengths of the filaments in a unit cube. Similarly the L_2 norm of vorticity is given by

$$L_2(\omega) = \int |\vec{\omega}|^2 \, dV$$
$$\propto \sum_{i=1}^{M} \sum_{j=1}^{N} dl_{ij}^2 \, Q_{ij}$$

3.2 e) Diagnostics – Energy Calculation

The total kinetic energy per unit cube was calculated approximately by using the velocities calculated on a 20 x 20 x 20 grid in the unit cube such that.

$$\text{kinetic Energy} = \frac{1}{2} \sum_{l=1}^{20} \sum_{m=1}^{20} \sum_{n=1}^{20} (u_1^2 + u_2^2 + u_3^2) h^3$$

$$h = 0.05$$

3.3 Beale and Majda Method for Periodic Lattice

3.3 a) Numerical Techniques

The two crosssed vortex filaments were discretized onto a grid of grid length h. For initial calculations the cross-sections of the filaments were limited to one grid point only and a value of vorticity was assigned to these points so that the circulation was equal to one for all the resolutions used, h = 0.05, 0.025, 0.0125 and 0.003125.

The three lowest resolution were run with boundaries 0 and 1 and the highest resolution with boundaries −0.5 and 0.5. The reason for the change was that some symmetry was lost due to rounding errors in the calculations.

For grid size h and a unit cube bounded by planes

$$\left.\begin{matrix} x_1 \\ x_2 \\ x_3 \end{matrix}\right\} = A \text{ and } 1+A,\ A = -0.5 \text{ or } 0$$

initial vorticities $\vec{\omega}_A(m)$ and $\vec{\omega}_B(m)$ were assigned to points $\vec{X}_A(m)$ on the first filament and $\vec{X}_B(m)$ on the second filament, respectively.

where
$$\vec{X}_A(m) = (x_1(m),\ x_2(m),\ 0.5+A-x_3(m))$$
$$\vec{X}_B(m) = (x_2(m),\ x_1(m),\ 0.5+A+x_3(m))$$
$$x_1(m) = A+0.5 \qquad m = 1, l+2 \text{ where } l = \frac{1.0}{h}$$
$$x_2(m) = (m-2)\times h + A$$
$$x_3(m) = nh \qquad n = \frac{0.05}{h}$$

and

$$\vec{\omega}_A(m) = (0, \omega_0, 0),\ \vec{\omega}_B(\omega_0, 0, 0) \text{ where } \omega_0 = \frac{1}{h^2}$$

No other points were required as the initial vorticity was along the filaments and hence only lengthwise derivatives of velocity were required. Again, the symmetry was used fully in the calculations, vorticity increments, velocities and positional increments were calculated for one filament and then used for the second filament as in Chorin's method. The same cutoff Rmax was used as in Chorin's method in order to limit the number of calculations required to find the velocities in a periodic domain and the nearest image was used if

Rmax < 0.5. There is a slight difference in that the distance tested in Chorin's method is between a node point and the midpoint of a segment

ie $$|\vec{a}^{\,in}_{jl}| = \left|\frac{1}{2}\left(\vec{x}c^{\,i}_{j'} + \vec{x}^{\,i}_{j}\right) - \vec{x}^{\,n}_{l}\right|$$

whereas in the Beale and Majda method the distance is between two grid points containing vorticity

eg $$|\vec{X}_A(m) - \vec{X}_A(k)|$$

This difference becomes more important when the minimum cutoff or filter function is applied as the distance is certain to be zero when m=k in the Beale and Majda method but will only be zero in Chorin's method in the exceptional case of the midpoint of a segment coinciding with a node or the length of a segment becoming zero. This was the reason for altering the cutoff in Chorin's method from $R_{min}^2 a$ to R_{min}^3.

to avoid testing for zero when using the same expression in the filter function in the Beale and Majda method.

Hence $$K_\delta(\vec{x}_i(t) - \vec{x}_j(t)) =$$

$$0 \quad \text{when} \quad |\vec{x}_i(t) - \vec{x}_j(t)| > R_{max}$$

$$-\frac{1}{4\pi}\frac{(\vec{x}_i(t) - \vec{x}_j(t))}{|\vec{x}_i(t) - \vec{x}_j(t)|^3} \quad \text{when} \quad R_{min} \leq |\vec{x}_i(t) - \vec{x}_j(t)| \leq R_{max}$$

$$-\frac{1}{4\pi}\frac{(\vec{x}_i(t) - \vec{x}_j(t))}{R_{min}^3} \quad \text{when} \quad |\vec{x}_i(t) - \vec{x}_j(t)| < R_{min}$$

4th order Runge-Kutta time integration was used, as in Chorin's method, for both the position and vorticity updates, as it was found to be the most stable integration scheme tried. A 2nd order centred difference was used for the velocity derivatives.

e.g.

$$\omega_i(\vec{x}(m), t-\Delta t) = \omega_i(\vec{x}(m), t) + \omega_i(\vec{x}(m), 0) \times \Delta t \times f \times \left\{ \frac{u_i(x(m+1), t) - u_i(x(m-1), t)}{2h} \right\}$$

where f is a factor depending on the time integration scheme used.

3.3 b) Diagnostics

The L_1 norm of vorticity was calculated as

$$\sum_m |\vec{\omega}_A(m)| h^3 + \sum_n |\vec{\omega}_B(n)| h^3$$

and the L_2 norm as

$$\sum_m |\vec{\omega}_A(m)|^2 h^3 + \sum_n |\vec{\omega}_B(n)|^2 h^3$$

The method of assigning the initial values of vorticity to the grid points meant that although the initial positions of some of the grid points coincided with some of the nodes in Chorin's methods, circulations were equivalent and initial L_1 norms were equivalent the L_2 norms were not equivalent. It is not clear as yet whether this has any major significance in the evolution of the vortex filaments.

The kinetic energy was estimated using the same method as for Chorin's scheme using the same 20 x 20 x 20 grid in a unit cube.

4. Results of Numerical Integrations

4.1 Chorin's method

a) Standard Integration

The standard integration, as described in section 3.2 a) used Rmin = 0.05, Rmax = 0.495, δ = 0.05, time step = 0.001 and a 4th order Runge-Kutta time integration scheme. The initial data had maximum resolution in regions of maximum stretching as determined by previous trial runs.

The initial configuration of the vortex filaments in a unit cube is shown in figure 4.1 a) and b) in a plan and side view, the symbols marking the node points. The two filaments become increasingly tangled, as each induces the other to move around it, and the evolution is shown in figures 4.2 a) and b), 4.3, 4.4 a) and b), 4.5 and 4.6.

After a slow initial increase in vorticity, until about 0.2 secs, there was then a rapid increase in both the L_1 and L_2 norms of vorticity such that, although there had only been approximately a 50% increase in vorticity by 0.2 secs, the L_1 norm was over 30 times its initial value when the integrations were stopped at 0.399 secs. The integrations were stopped when each filament had 999 segments produced from the 160 initial segments. The evolution of the L_1 norm of vorticity is shown in figure 4.7 and table 4.1 and that of the L_2 norm in table 4.3.

If the vorticity is to become singular in a finite time the rate of increase of the L_1 norm of vorticity must be greater than an exponential increase.

Hence by considering

$$L'_1(\omega,t) = L'_{10}(\omega,0)\exp(t/\tau)$$

where τ is constant

$$\frac{dL'_1(\omega,t)}{dt} = \frac{L'_1(\omega,t)}{\tau}$$

$$R = \frac{dL'_1(\omega,t)}{dt} \Big/ L_1(\omega,t) = \frac{1}{\tau} = \text{constant}$$

If the ratio of the rate of change of the L_1 norm to the L_1 norm increases with time the vorticity is increasing at a rate faster than exponential. By considering table 4.2 it is seen that the ratio increases until about 0.26 sec when it becomes roughly constant, until approximately 0.36 secs when it begins increasing again. These results are confirmed when the resolution of the 0.001 timesteps is used. Obviously further integrations are required if the trend is to be established. The variation of the rate of increase of the L_1 norm may be linked to the intermittency observed by Chorin (1982) or may be due to the decreasing accuracy of the solution due to rounding errors and errors inherent in the method.

This obviously needs further study and although the results suggest that the vorticity is tending to a singularity they are not conclusive.

Table 4.3 and figure 4.8 show the variation of the maximum and minimum segment radii with time. If the minimum radius is a measure of the smallest scale of the motion there is a scale collapse of almost 3 orders of magnitude in the integration period. However since the cutoff Rmin is constant and determines the velocity field it is felt that the minimum radius may not be a very good measure of the scale of motion but this needs to be checked by considering fourier analysis of

the velocity field. The fourier analysis is not straight forward due to the nature of the velocity field induced by the vorticities since the gradient contains a discontinuity at distance Rmin from a filament and hence even the initial field contains an infinite number of modes. This makes it difficult to distinguish signals due to small scale vorticity, especially since, as seen in figure 4.9, the smallest scales occupy only a small fraction of the total volume occupied by vorticity. However the radius is a measure of the stretching that has occurred since, as the radius decreases from r to xr the segment length increases from l to $\frac{l}{x^2}$.

By the end of the integration period a very small fraction of the filaments have stretched by a factor of more than 10^5 whereas other parts have been compressed slightly. As shown in figure 4.9, the most highly stretched segments with high enstrophy (L_2 norm of vorticity) occupy a very small fraction of the total volume, again an indication of intermittency.

One test of the stability of the method is the conservation of kinetic energy. It should be possible to calculate this from the vorticity distribution directly using the equation

$$K.E. = \frac{8}{8\pi} \iint \frac{\vec{\omega} \cdot \vec{\omega}'}{|\vec{x} - \vec{x}'|} dV(\vec{x}) dV(\vec{x}')$$

However, I have not found a form consistent with the cutoff applied to the velocity field calculations, so the approximation of calculations on a 20^3 grid has been used. As seen from table 4.4 a) the kinetic energy is roughly conserved. The conservation of energy, despite rapidly increasing vorticity, is achieved as described by Chorin (1982) by pairing of opposite signed vorticity such that the velocity fields

cancel. In this case it can be achieved either by two parts of the same filament or the two separate filaments in a unit cube, lining up. This is illustrated in figure 4.6 where the solid and dashed lines mark the two separate vortex filaments in a unit cube and the arrow heads mark the direction of the vorticity. It is felt that maybe the vortex pairing is in part responsible for the rapid increase in the L_1 norm. A pair of rectilinear line vortices will induce motion on each other such that they will move in a direction normal to the line joining their axes (see Batchelor pg 534) and hence sections of paired filaments could move causing stretching at the end of the paired section. Thus the detailed interactions of vortices may be important for correct modelling of vorticity, especially in the viscous case, where it may be possible that paired sections merge removing vorticity from the fluid.

b) Constant length initial segments DLI = 0.05

Initially the integrations were run with all the same parameters as in the standard case but with all the initial segments of the same length, 0.05. However after running tests with increased resolution it was seen that the segment splitting could not reproduce the curvature of the filaments well when $\ell = 0.05$, see figure 4.10 a) as compared with figure 4.2a). This was the reason for the variable length segments used in the standard integration. Table 4.1 shows that the evolution of the L_1 norm agrees well with the standard case until about 0.3 secs when the constant case L_1 norm begins to increase more rapidly, probably due to increasing errors resulting from the lack of resolution. Figure 4.10 b) shows that the configuration of the filaments is also different from that of the standard integration,

figure 4.4 a) by 0.35 secs. Table 4.4 a) also shows that the energy is greater than the standard case for most of the integration period, however it is still roughly conserved.

c) Increasing the maximum cutoff, Rmax = 0.995

In order to test the sensitivity of the results to the approximation to periodicity the maximum separation of points included in the calculation of velocity was increased to 0.995 from 0.495. This means that more 'images' are included in the calculation and as Rmax tends to infinity the solution will tend to the correct solution for periodic data. The results are very similar to those from the standard case, indicating that the smaller cutoff, used to reduce the number of calculations required, is a good approximation to periodic boundary conditions. The evolution of the L_1 norm of vorticity, compare table 4.1 and 4.5 a), shows that the increase with time is slightly less in the case of Rmax = 0.995 but the trends are the same. Table 4.5 b) shows that the kinetic energy is again roughly conserved. The general features of the filament configurations are the same, such as the pairing of filaments, although the actual positions are slightly different.

d) Simpler time integration schemes

In order to try to decrease the CPU time required for the integrations simpler time integration schemes were tried, such as centred difference and Euler forward difference. This also tested the consistency of the solutions as trials with Chorin's turbulent vortex data, see the introduction, section 3.1 and figure 3.1, showed that the solution depended on the exact scheme and size of time steps used. All schemes agreed well until approximately 0.2 secs, see table 4.6. Time

splitting occurs in the centred difference scheme solution which becomes evident as an oscillation in the maximum node point velocity by 0.274 secs and in the L_1 norm of vorticity by 0.312 secs, the amplitude increasing until the calculations were stopped at 0.365 secs when 999 segments had been produced on each filament. By the time the instability was evident the solution was diverging from that obtained from the more accurate 4th order Runge-Kutta time integration scheme. The instability is also shown by an increase in the calculated kinetic energy, see table 4.4 a), supporting the use of the conservation of the calculated value as a measure of stability and correctness of a given solution. The stability of the centred difference scheme is improved by using a time filter such that

$$\vec{x}^{n+1} = (1-\xi)\left(\vec{x}^{n-1} + 2 \times dt \times \vec{u}(\vec{x}^{n})\right) + \xi\left(2\vec{x}^{n} - \vec{x}^{n-1}\right)$$

where n indicates the time level and ξ is a weighting factor. This is equivalent to a weighted average of the centred time difference solution and the solution such that $\vec{x}^{n}$ is the mean of $\vec{x}^{n+1}$ and $\vec{x}^{n-1}$ Using $\xi = 0.1$, good agreement is found with the fourth order Runge-Kutta solution and with no obvious signs of oscillation by 0.399 secs. There are signs of an increase of kinetic energy by the end of the integration period, so the solution may not be reliable in further integrations, see table 4.4a.

The Euler first order forward difference time integration scheme, as used by Chorin (1982) diverges from the standard solution by the end of the integration period, by which time the kinetic energy is also increasing, indicating that the solution cannot be trusted.

These tests show the reproducibility of the solution whilst kinetic energy is conserved.

e) Decreasing maximum segment length, ℓ

Test runs to 0.3 secs show reproducibility of the solution when ℓ is decreased. With all other parameters as in the standard solution, the maximum segment length allowed was decreased to 0.025 and 0.0125 from 0.05. This should allow greater resolution of curvature and this was in fact seen in the plots of the filament configurations, the general shape being the same. The vorticity norms were slightly less with the greater resolution, the L_1 norm of vorticity being 13.2, 13.0 and 12.6 after 0.3 secs, decreasing with increasing resolution. For the case with highest resolution the solution agreed with the standard integration until about 0.16 secs and then the rate of increase of the L_1 norm was slightly lower.

f) Increasing time step dt

Trial integrations with increased time steps also gave results consistent with the standard integration. Time steps of 0.005 and 0.0025 have been tried, the L_1 norm of vorticity at a given time, after about 0.34 secs, increasing only slightly with decreasing time resolution.

g) Changing the form of the smoothing function $\psi(a)$

The various tests of Chorin's method described above show that the standard integration performed for the periodic lattice data produces a solution, only weakly, dependent on the values of dt, ℓ, Rmax, the time integration scheme and the resolution of the initial data. However, various runs with different forms of the smoothing function do show marked differences as described below.

In order to test the validity of the use of the filament radius as a measure of the scale of motion a trial integration was run with the value of Rmin allowed to vary with the radius of the segments, each segment used in the velocity calculations having a radius determined from the amount of stretching undergone, see section 3.2c, at a given time.

The function ψ (a) was then of the form

$$\psi_j(a) = \begin{cases} \infty & |a| > R_{max} \\ |a|^3 & R_{min_j} \leq |a| \leq R_{max} \\ R_{min_j}^3 & |a| < R_{min_j} \end{cases}$$

where R_{min_j} = radius of jth segment.

Initially radius of all segments = R_{min_j} = 0.05.

The reason for this change was that it was felt that when Rmin is kept constant the vortex interactions are mistreated, reducing the effect of vortex stretching on strain rates. The strain rate can only increase due to the presence of more vorticity in the fluid since the effect of increased velocities near filaments, due to the production by stretching of intensified vorticity inside a smaller cross-section is removed. Thus smaller scale structure, due to variable amounts of stretching along the filament, may be lost, possibly introducing some viscosity.

The results showed a far more rapid increase in vorticity, see table 4.5a), than for the standard integration. The integrations have not been followed for a long period of time as yet because the far higher induced velocities on the filament mean that the time step is also rapidly reduced. The evolution is similar to the standard integration until about 0.15 secs, then the maximum induced velocity of

the filaments increases from a value of 1.6 ms^{-1}, approximately the initial value, to 28 ms^{-1} by 0.197 secs and to 347 ms^{-1} by 0.224 secs the end of the integration. The standard integration does show an increase in velocity after 0.15 secs and reaches 4 ms^{-1} by 0.2 secs as the two filaments approach each other, but the velocity only reaches a maximum of 5.19 ms^{-1} after 0.333 secs and has reduced to 4.7 ms^{-1} by the end of the integration period, 0.399 secs, there being oscillations of varying periods and amplitudes during the period. These velocities can be understood by considering the induced velocity field of a straight line vortex given by

$$|\vec{u}(a)| = \frac{\Gamma}{2\pi a}$$

where a is the radial distance

Γ is the circulation

which increases with decreasing a, see Batchelor pg 94. When the cutoff R_{min}^3 is used the velocity field decreases with a inside the 'radius' Rmin to zero on the vortex. Thus the theoretical maximum velocity, ignoring the effects of curvature, in this case will be $\frac{1}{2\pi R_{min}}$ This is equal to 3.18 for Rmin = 0.05 and rises to 22 for the minimum radius after 0.197 secs and 128 for the minimum radius by the end of the integration. Obviously the approximations of the method will also produce slightly different values for the velocities than theory predicts. The increase in velocities and vorticity in the case when Rmin is allowed to vary according to the stretching of individual segments is apparently a result of 'pairing' of opposite signed vorticity, as described earlier, producing stretching but this time producing higher velocities, and hence more stretching than in the standard integration, due to the closeness of the two sections of

filaments. This suggested mechanism for the rapid production of vorticity requires further study, maybe a uniform value of Rmin should be used for the whole filament if internal waves smooth out variations along the length, Moore and Saffman (1972). Chorin (1982) using $\psi(a) = Rmin^2 a$ states that when Rmin was allowed to vary, as in this case, the results were the same as for the case with constant Rmin if the timestep, δ and Rmax were adjusted. The other parameters have not been varied in this case and will be in future studies since the value of δ in this case is larger than the reduced values of Rmin at later times, which may be an unstable situation, also the segments either side of a node point do not contribute to the velocity induced at that point and hence, if the value of δ is larger than Rmin, it may remove important contributions to the velocity calculations.

One further observation in this case is that the kinetic energy, see table 4.5 b), has increased by 0.197s so the calculations may be becoming unreliable.

A final test integration of Chorin's method used his form of the function $\psi(a)$

$$\psi(a) = \begin{cases} \infty & |a| > Rmax \\ |a|^3 & Rmin \leq |a| \leq Rmax \\ Rmin^2 |a| & |a| < Rmin \end{cases}$$

with Rmin = 0.05 = constant as before.

Again the evolution is similar to the standard integration until about 0.15 secs when the L_1 and L_2 norms of vorticity increase more rapidly than in the standard integration, reaching 999 segments per filament and an L_1 norm similar to that in the standard integration by 0.34 secs. Again vortex pairing is observed, although the

configuration is different from the standard integration. The kinetic energy, see figure 4.5 b), is again increasing by the end of the integration so the results may not be reliable.

Obviously the results of these integrations show that the evolution of the flow is dependent on the form of the function $\psi(a)$. This function, certainly in the case where only one filament represents a vortex, contains the only information concerning the internal structure of the vortex. Trials with a vortex ring configuration, with non-periodic boundaries, indicate that if the resolution is sufficiently high, that is sufficiently small segments lengths the resultant velocities of translation of the ring approximate those of a ring with uniform vorticity distribution in a cross-section of radius Rmin for a given ring radius. Hence the value of Rmin appears to represent the value of the radius of the vortex. The assumed value of 0.025 mentioned in section 3.1 and table 4.3 doesn't affect the calculations at all for the vortex lattice data with Rmin = 0.05, all future radii just being scaled as the initial radius and Rmin. The form of the function ψ (a) in the standard integration does not in fact represent a uniform distribution of vorticity but one increasing from zero at $|a|$ = Rmin to $\frac{3}{2\pi Rmin^2}$ at $|a|$ = zero

The form of the distribution is

$$\omega(|a|) = \frac{3}{2\pi Rmin^3}\sqrt{Rmin^2 - |a|^2}$$

Chorin's function ψ (a) in fact represents a distribution increasing from zero at Rmin and becoming infinite on the line segments. It may be possible that by keeping Rmin constant some diffusion is being added to the problem, counteracting the rapid increase of vorticity.

4.2 Beale and Majda's Method

As the resolution along the filaments is increased the configuration of the filaments appears to be converging to that produced by Chorin's method as can be seen by comparing figures 4.11, 4.12, 4.13 and 4.14 with figure 4.2 a). However the resolution appears to be unable to deal with the rapid increase in vorticity after about 0.2 secs and the solutions diverge as can be seen in table 4.1, figure 4.7 and the comparison between figures 4.15 to 4.17 and figures 4.3 to 4.5. The solutions are able to follow the solution from the standard integration of Chorin's method for longer periods into the integration as the resolution is increased, the case with $h = 0.003125$ almost matching the standard integration out to 0.25 secs. The L_1 norms of vorticity show a smaller increase by 0.4 secs than with Chorin's method, although the increase in the L_1 norm with resolution seems to indicate that the solutions are converging to that obtained by Chorin's method.

The variations of kinetic energy with time, shown in table 4.4 b), do not provide conclusive evidence to support convergence. It was hoped that as the resolution increased the kinetic energy would not increase as rapidly with time. However there are no definite trends in that sense, although all four cases do show an increase in kinetic energy with time indicating instability.

These results provide evidence to support the accuracy of the solution obtained by Chorin's method but they do introduce a problem concerning exactly what situation is being modelled. The solutions of the Beale and Majda integrations may be converging to the singular solutions for infinitely thin vortex filaments, since, as the

resolution along the length of the filament is increased the cross-section is reduced, in order to have only one grid-point in the cross-section with a uniform grid. In the limit of infinite resolution, the cross-section will be infinitesimal and contain infinite vorticity, as the circulation is kept equal to one. However, as discussed earlier the value of Rmin and the functions $\psi(a)$ or $K(x)$ may override the effective resolution 'cross-section' and provide more important information on the radius of the vortex and the distribution of vorticity. Alternatively the solution may only depend on the circulation, set equal to one for all cases, when the cross-section is small compared with the periodic length scale of separation of the filaments.

5. Conclusions

The results from the integrations using Chorin's three dimensional vortex produce a solution only weakly dependent on the time integration scheme, time step, resolution of initial data, maximum segment length and the maximum separation of segments from nodes. However the value of the distance at which the function $\psi(a)$ changes form and the form of the function that is used close to the filaments does appear important when one filament represents a vortex. The calculations need to be extended to increase resolution in the cross-section, core, of the vortices, so that a single vortex is represented, by a bundle of filaments. This will aid understanding of the situation being modelled by a single filament with a given function $\psi(a)$ and value of Rmin. Initial trials with a bundle of five or seven filaments per vortex produce extra vorticity due to twisting of the outer filaments around a central one on the axis of the vortex when Rmin is of the order of the spacing of the filaments eg spacing and segment

length = 0.0125, Rmin = 0.0187. When Rmin was much larger than the spacing, Rmin = 0.05, spacing and initial segments lengths = 0.0125, the twisting is suppressed but the solution is not the same as for the standard integration described here. Further study is required to investigate the interactions between the searate filaments in a bundle to ensure that a bundle does not act as separate vortices.

The results from the integrations using Beale and Majda's method converge towards those obtained by Chorin's method as the resolution is increased, supporting the accuracy of Chorin's method but raising the problem of whether the intiial data being represented is in fact singular.

The evolution of the periodic lattice of vortex filaments shows a rapid increase with time of the L_1 and L_2 norms of vorticity. This indicates the presence of a singularity in finite time but the results are not conclusive as discussed in section 4.1 a). The lattice is constrained by periodicity to keep its basic shape but as the vorticity increases a greater region of space contains some vorticity, although the actual volume of fluid containing vorticity remains constant. These results support the work of Chorin (1981, 1982) but raise the aspect that it is important to consider their importance if, in fact, the initial data is singular.

An apparent scale collapse of almost three orders of magnitude is obtained by the end of the integration period but as discussed in section 4.1 a) the importance may not be valid with the particular form of $\psi(a)$ that has been implemented.

Possibly the most important product of this study is that the mechanism of 'vortex pairing', identified by Chorin (1982) as being necessary in order to conserve energy, may in fact be responsible for the

rapid increase in vorticity. This thus identifies the need for detailed consideration of vortex interactions in the implementation of three dimensional vortex methods.

References

Batchelor, G. K. 'An introduction to Fluid Dynamics', Cambridge University Press, 1967.

Beale J. T. and Majda, A. 1982(a), 'Vortex Methods. I: Convergence in Three Dimensions', Math. Comp. 39.

Beale J. T. and Majda, A. 1982 (b) 'Vortex Methods. II: Higher Order Accuracy in two and Three dimensions', Math. Comp 39.

Beale J. T. and Majda, A. J. 1983 'Explicit Smooth Velocity kernels for Vortex Methods' MRC Tech. Summary Report No. 2480 University of Wisconsin.

Brachet, M. E., Meiron, D. I., Orszag, S. A., Nickel, B. G., Morf, R. H. and Frisch, U. 1983 'Small Scale Structure of the Taylor-Green Vortex', J. Fluid Mech. 130, 411-452.

Chorin A. J. 1981 'Estimates of Intermittency, Spectra and Blow-up in developed Turbulence' Communs Pure Appl Maths 34 853-866.

Chorin A. J. 1982 'The Evolution of a Turbulent Vortex' Commun Math Phys 83 517-536.

Cullen M. J. 1983 'Current Progress and Prospects in Numerical Techniques for Weather Prediction Models' J. Compt. Phys 50 1-37.

Hald, O. 1979 'The Convergence of vortex Methods, II' SIAM J. Numer. Anal. 16, 726-755.

Holt, M. W. 1982 'A Program to Implement the 3-D Vortex Algorithm of Beale and Majda' Met O 11 Working Paper No 45.

Leonard, A. 1980 'Vortex Methods for Flow Simulations' J Comput. Phys. 37, 289-335.

Mandelbrot B.1972 in 'Statistical Models and Turbulence' Rosenblatt M. Van Atta C, (eds), 333-358, Berlin, Heidelberg, New York: Springer.

Mandelbrot B.1974 'Intermittent Turbulence in Self-Similar Cascades: Divergences of High Moments and Dimension of the Carrier', J. Fluid Mech, 62, 331-358.

Milne-Thomson, L. M. 1968 'Theoretical Hydrodynamics', Macmillan & Co, 1968 pg. 84.

Moore D W and Saffman P. G. 1972 'The Motion of a Vortex Filament with Axial Flow', Phil. Trans. Roy. Soc. 272, 403-429.

Morf, R. H., Orszag, S. A. and Frisch U. 1980 'Spontaneous singularity in Three Dimensional, Inviscid, Incompressible flow' Phys. Rev. Lett. 44, 572-575.

Figure Captions

Figure 2.1 Vortex segment

Figure 3.1 Chorin's initial data for turbulent vortex.

Figure 3.2 Initial data for lattice of vortex filaments.

Figure 4.1a) Plan view of initial data in standard integration using Chorin's method.

——— 1st filament X initial nodes on 1st filament

— — —. 2nd filament O initial nodes on 2nd filament.

Figure 4.1b) Side view of initial data in standard integration using Chorin's method.

Figure 4.2a) Plan view after 0.2 secs for standard integration using Chorin's method.

Figure 4.2b) Side view

Figure 4.3 Plan view after 0.25 secs for standard integration using Chorin's method.

Figure 4.4a) Plan view after 0.35 secs for standard integration using Chorin's methods.

Figure 4.4b) Side view.

Figure 4.5 Plan view after 0.398 secs for standard integration using Chorin's method.

Figure 4.6 3-D representation of configuration of the vortex filaments after 0.398 secs for standard integration using Chorin's method.

——— 1st filament ▶ direction of vorticity

— — — 2nd filament

Figure 4.7 Evolution of L_1 norm of vorticity for vortex filaments.

Figure 4.8 Evolution of core radius (stretching) from Chorin's method.

Figure 4.9 Histograms of enstrophy and volume per 0.1 interval of $\log_{10}$ (radius) after 0.398 secs from Chorin's method.

Figure 4.10a) Plan view after 0.2 secs for initial segments of equal length of 0.05 using Chorin's method.

Figure 4.10b) Plan view after 0.35 secs for initial segments of equal length of 0.05 using Chorin's method.

Figure 4.11 Plan view after 0.2 secs for Beale and Majda's method

$H = 0.05$

0 vorticity component into paper, + vorticity component out of paper

⟶ magnitude and direction of vorticity scaled so that initial magnitude = H.

Figure 4.12 As figure 4.11 but $H = 0.025$.

Figure 4.13 As figure 4.11 but $H = 0.0125$.

Figure 4.14 As figure 4.11 but $H = 0.003125$ and symbols denoting component of vorticity in Z direction removed for clarity.

Figure 4.15 As figure 4.14 but after 0.25 secs.

Figure 4.16 As figure 4.14 but after 0.35 secs.

Figure 4.17 As figure 4.14 but after 0.4 secs.

TIME	L_1 Norm of Vorticity					
	CHORIN		BEALE AND MAJDA			
	Variable DLI	DLI=0.05	H=3.125x10^{-4}	H=0.0125	H=0.025	H=0.05
0	2.0	2.0	2.0	2.0	2.0	2.0
0.02	2.008	2.008	2.008	2.008	2.008	2.006
0.04	2.032	2.032	2.033	2.032	2.031	2.026
0.06	2.072	2.072	2.073	2.071	2.068	2.06
0.08	2.12	2.12	2.12	2.12	2.12	2.10
0.10	2.18	2.19	2.19	2.18	2.18	2.16
0.12	2.26	2.28	2.26	2.25	2.24	2.21
0.14	2.36	2.39	2.35	2.34	2.33	2.26
0.16	2.5	2.55	2.48	2.44	2.42	2.32
0.18	2.74	2.83	2.68	2.6	2.54	2.41
0.2	3.22	3.34	3.11	2.86	2.71	2.5
0.22	4.14	4.17	3.94	3.32	2.92	2.62
0.24	5.38	5.34	5.02	3.88	3.16	2.72
0.26	7.06	7.01	6.18	4.57	3.42	2.84
0.28	9.7	9.48	7.51	5.35	3.71	2.94
0.3	13.2	13.3	9.1	5.95	4.08	3.08
0.32	17.9	18.6	11.6	6.62	4.43	3.26
0.34	24.2	26.4	14.6	7.54	4.53	3.46
0.36	33.2	38.2	18.3	8.04	4.56	3.66
0.38	46.5	53.96	23.1	8.3	4.59	3.86
0.39	55.8	64.32				
0.392		66.76				
0.395	61.2					
0.399	66					
0.4			28.4	9.2	4.67	4.04

Table 4.1 Evolution of L_1 Norm of Vorticity

All integrations used 4th order Runge-Kutta time integration scheme with time step 0.001. Maximum cutoff Rmax = 0.495, Rmin = 0.05 and minimum cutoff function $\psi(a) = Rmin^3$.

Time t	L_1 norm of vorticity	dL_1 L_1 (t+0.02) − L_1 (t−0.02)	$\frac{dL_1}{dt} \times L_1$
0.02	2.008	0.032	0.398
0.04	2.032	0.064	0.787
0.06	2.072	0.088	1.06
0.08	2.12	0.108	1.27
0.1	2.18	0.14	1.61
0.12	2.26	0.18	1.99
0.14	2.36	0.24	2.54
0.16	2.5	0.38	3.8
0.18	2.74	0.72	6.57
0.2	3.22	1.4	10.8
0.22	4.14	2.16	13.0
0.24	5.38	2.92	13.6
0.26	7.06	4.32	15.3
0.28	9.7	6.14	15.8
0.3	13.2	8.2	15.5
0.32	17.9	11.0	15.4
0.34	24.2	15.3	15.8
0.36	33.2	22.3	16.8
0.38	46.5	32.8*	18.1

* L_1 (0.399) − L_1 (0.36)

Table 4.2 Evolution of $\frac{dL_1}{dt} / L_1$ to compare rate of increase of L_1 norm of vorticity with exponential rate.

If rate of increase of L_1 norm of vorticity is exponential

$$L_1 = L_{10} \exp(t/\tau)$$

$$\frac{dL_1}{dt} = \frac{L_1}{\tau}$$

$$\frac{dL_1}{dt} / L_1 = \frac{1}{\tau} = \text{constant}$$

Time	4th order Runge-Kutta	Centred Difference	Euler Forward Difference	Centred Difference with filtering	4th order Runge-Kutta	
	varying length initial segments, minimum DLI = 0.05/128					DLI=0.05
	Rmax=0.495	Rmax=0.495	Rmax=0.495	Rmax=0.495	Rmax=0.995	Rmax=0.495
0.0	0.351	0.351	0.351	0.351	0.323	0.349
0.1	0.341	0.341	0.341	0.34	0.314	0.343
0.2	0.330	0.330	0.330	0.330	0.305	0.337
0.3	0.335	0.337	0.339	0.334	0.309	0.345
0.35	0.330	0.549	0.352	0.340	0.308	0.341
0.36	0.332	0.823				
0.37	0.334		0.355	0.343	0.319	0.343
0.38	0.337		0.370	0.342	0.324	0.350
0.39	0.340		0.380	0.350	0.322	0.352
0.395	0.338					
0.398	0.337					
0.399					0.320	

Table 4.4 a) Kinetic energy as calculated on a 20 x 20 x 20 grid in a unit cube for Chorin's Method.

Time	4th order Runge-Kutta time integration Rmax = 0.495			
	H = 0.003125	H = 0.0125	H = 0.025	H = 0.05
0	0.351	0.351	0.351	0.354
0.05	0.340	0.342	0.342	
0.1	0.339	0.341	0.340	0.341
0.15	0.334	0.336	0.335	0.339
0.2	0.326	0.330	0.330	0.339
0.25	0.329	0.339	0.333	0.338
0.3	0.373	0.402	0.339	0.342
0.35	0.617	0.479	0.368	0.362
0.4	1.70	0.540	0.384	0.420

Table 4.4 b) As table 4 a) but for Beale and Majda's Method

Time	L_1 Norm of Vorticity		
	CHORIN		
	$\psi(a)=Rmin^3$ Rmin=0.05 Rmax=0.995	$\psi(a)=Rmin^2a$ Rmin=0.05 Rmax=0.495	$\psi(a)=Rmin^3$ Rmin=Radius Rmax=0.495
0	2.0	2.0	2.0
0.02	2.008	2.008	2.008
0.04	2.029	2.032	2.032
0.06	2.066	2.07	2.07
0.08	2.12	2.12	2.12
0.1	2.18	2.18	2.17
0.12	2.24	2.26	2.24
0.14	2.32	2.35	2.31
0.16	2.46	2.50	2.41
0.18	2.66	2.82	2.60
0.2	3.08	3.69	3.26
0.22	3.92	5.2	8.3
0.24	5.14	7.2	12.5[+]
0.26	6.86	10.1	
0.28	9.38	15.1	
0.3	12.4	24.1	
0.32	16.7	38.8	[+]at 0.224
0.34	22.8	65.3	(247 segments)
0.36	31.1		
0.38	43.0		
0.39	51.4		
0.395	56.4		
0.399	60.8		

Table 4.5 a) Evolution of L_1 norm of vorticity for Chorin's method with different Rmax and smoothing functions $\psi(a)$.

Table 4.5 b) Evolution of kinetic energy for cases in Table 4.5(a)

	ψ (a) = Rmin^3 Rmin = 0.05 Rmax = 0.995	ψ (a) = Rmin^{2}a Rmin = 0.05 Rmax = 0.495	ψ (a) = Rmin^3 Rmin = Radius Rmax = 0.495
Time	Kinetic Energy		
0.0	0.323	0.351	0.351
0.1	0.314	0.353	0.356
0.197			0.373
0.2	0.305	0.345	
0.3	0.309	0.361	
0.34		0.386	
0.35	0.308		
0.37	0.319		
0.38	0.324		
0.39	0.322		
0.399	0.320		

Time	4th order Runge-Kutta		Centred Difference		Euler Forward Difference		Centred Difference with Filtering = 0.1	
	L_1	L_2	L_1	L_2	L_1	L_2	L_1	L_2
0	2.0	1.02x 10^3	2.0	1.02x 10^3	2.0	1.02x 10^3	2.0	1.02x 10^3
.04	2.032	1.1 x 10^3	2.032	1.1 x 10^3	2.032	1.1 x 10^3	2.032	1.1 x 10^3
.08	2.12	1.3 x 10^3	2.12	1.3 x 10^3	2.12	1.3 x 10^3	2.12	1.3 x 10^3
.12	2.26	1.6 x 10^3	2.26	1.6 x 10^3	2.26	1.6 x 10^3	2.26	1.6 x 10^3
.16	2.5	2.1 x 10^3	2.5	2.1 x 10^3	2.5	2.1 x 10^3	2.5	2.1 x 10^3
.2	3.22	5.2 x 10^3	3.22	5.1 x 10^3	3.18	4.6 x 10^3	3.22	5.1 x 10^3
.24	5.38	4.0 x 10^4	5.4	4.0 x 10^4	5.24	3.6 x 10^4	5.38	4.0 x 10^4
.28	9.7	2.0 x 10^5	9.7	2.0 x 10^5	9.1	1.9 x 10^5	9.58	2.1 x 10^5
.32	17.9	1.0 x 10^6	19.1	1.2 x 10^6	17.6	1.1 x 10^6	17.8	1.0 x 10^6
.36	33.2	5.8 x 10^6	51.0	1.5 x 10^7	36.4	9.5 x 10^6	33.2	6.1 x 10^6
.365	36.0	7.5 x 10^6	58.2	2.2 x 10^7	40.0	1.2 x 10^7	36.1	7.6 x 10^6
.391	57.7	3.1 x 10^7			66.8	5.1 x 10^7	57.1	2.5 x 10^7
.399	66.0*	5.3 x 10^7					65.9	3.6 x 10^7

Table 4.6 Evolution of L_1 and L_2 norms of vorticity for Chorin's method with different time integration schemes.

Figure 2.1

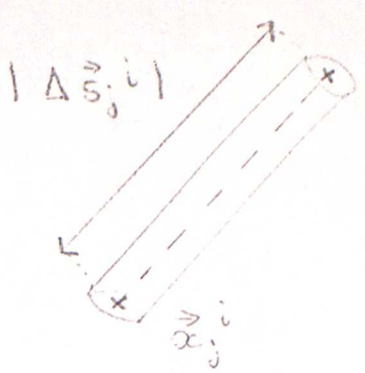

Vortex segment j of filament i

Figure 3.1

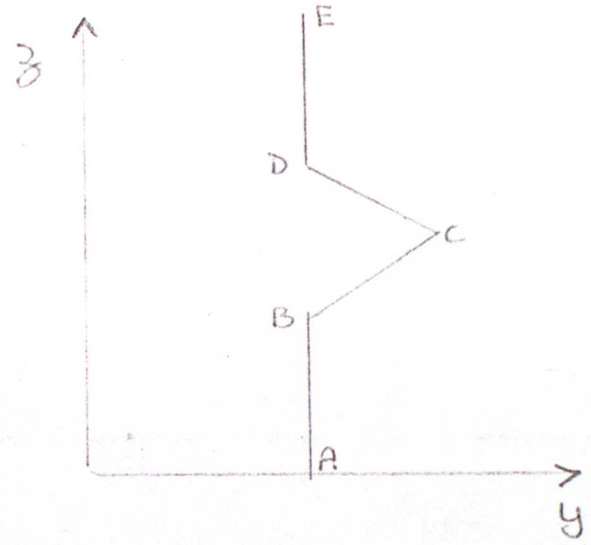

A = (0.5, 0.5, 0)
B = (0.5, 0.5, 0.4)
C = (0.5, 0.6, 0.6)
D = (0.5, 0.5, 0.8)
E = (0.5, 0.5, 1.0)

Figure 3.2

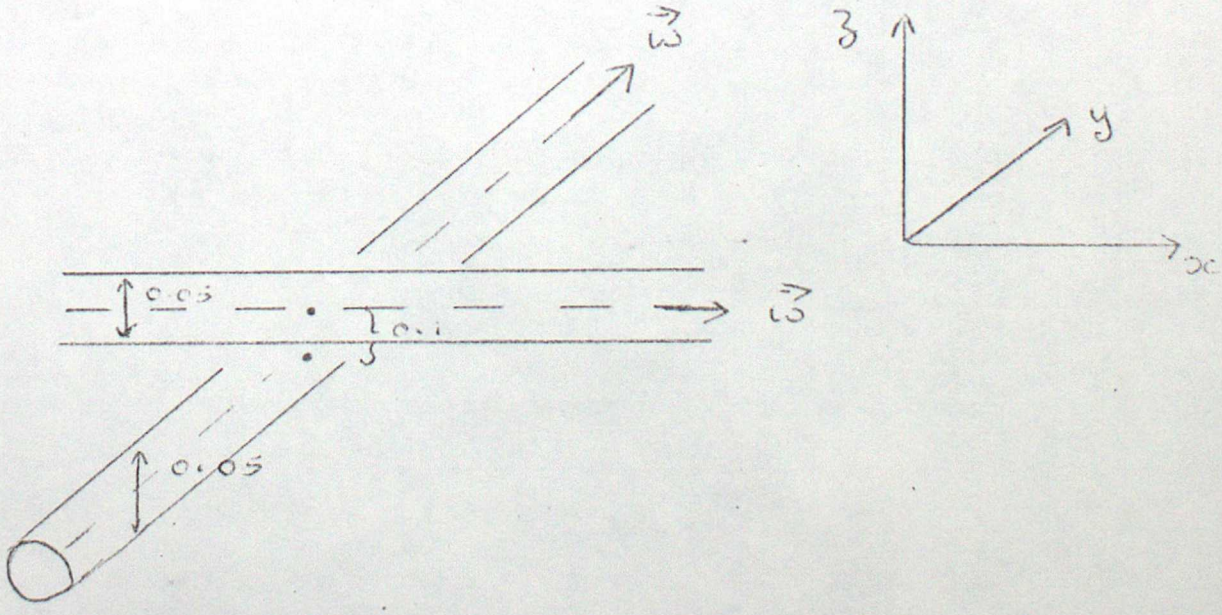

Figure 4.1a)

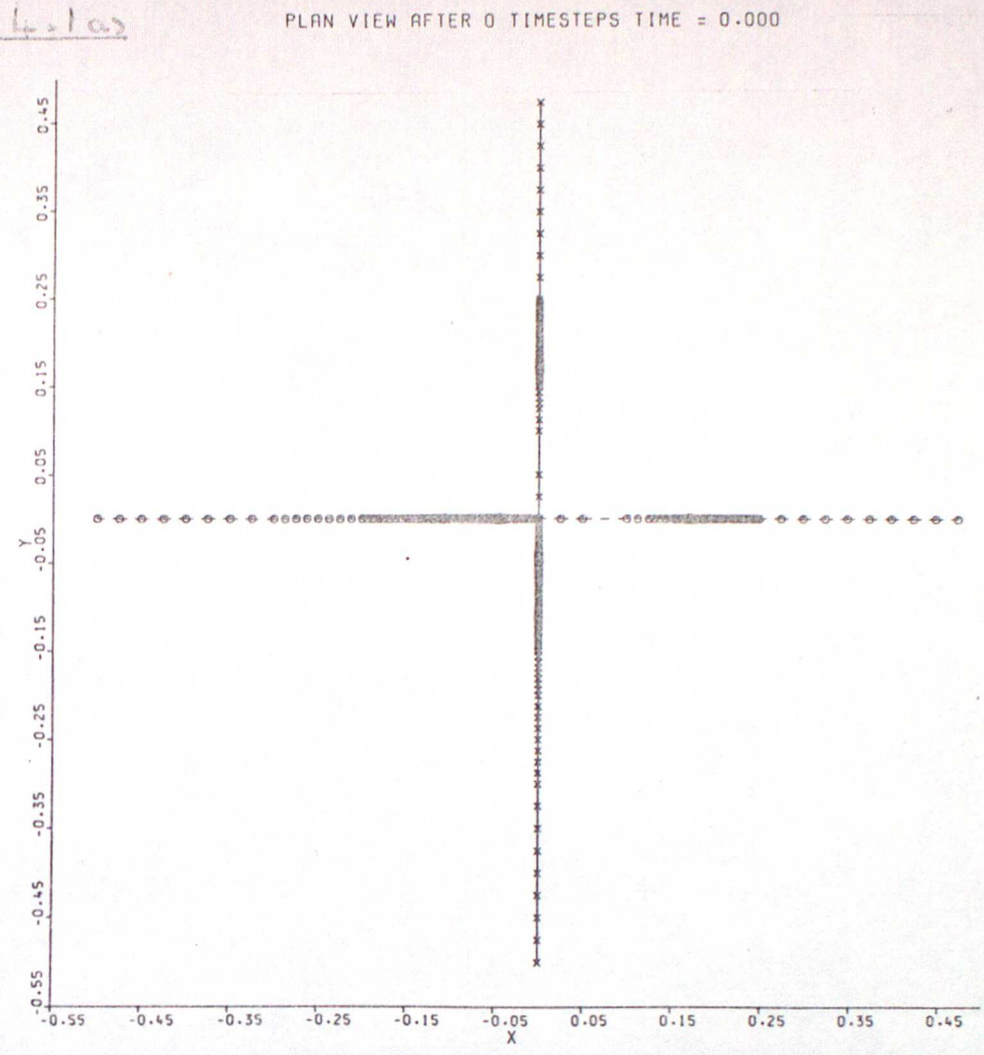

Figure 4.1b)

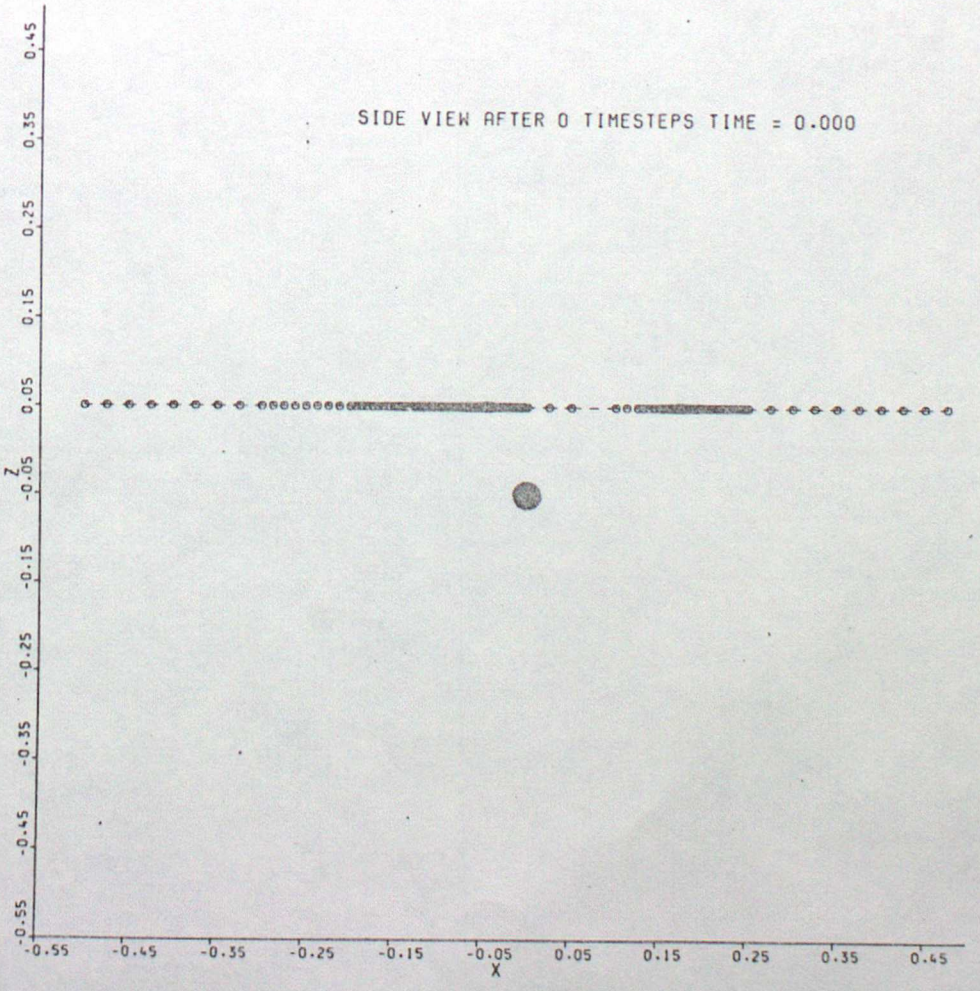

Figure 4.2a)

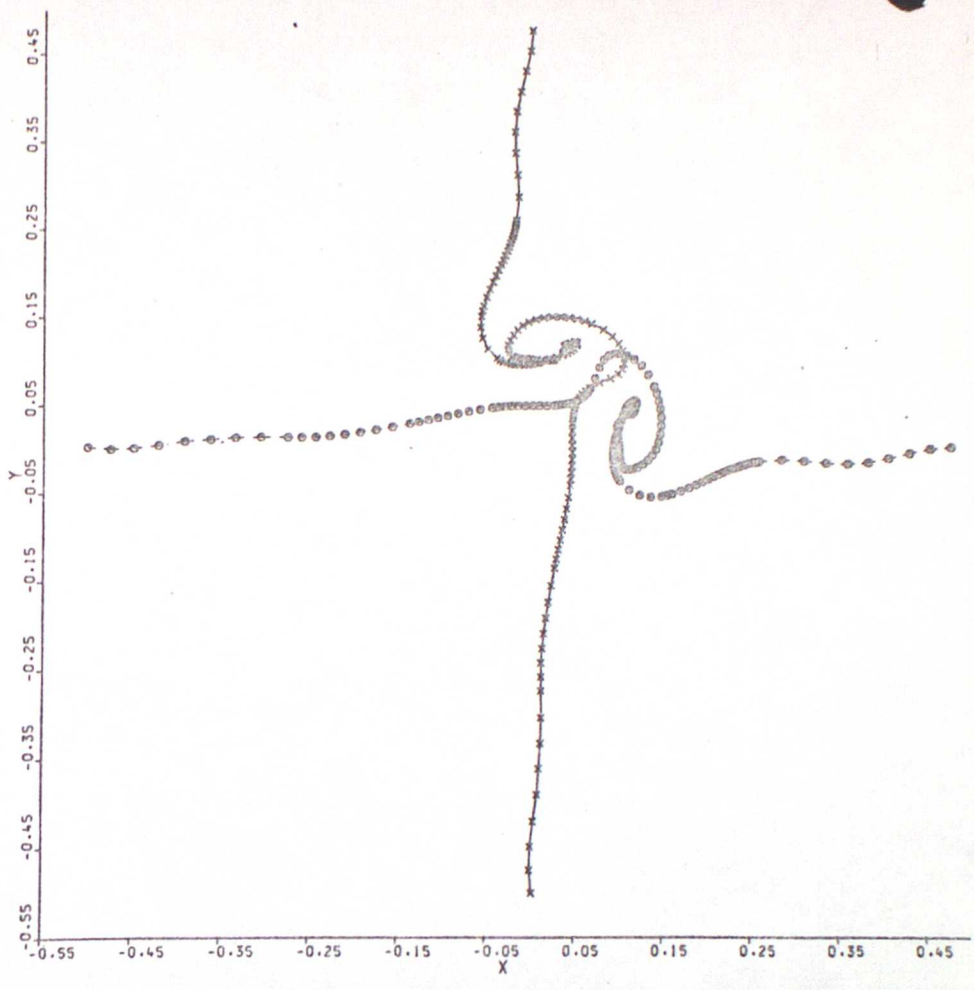

Figure 4.2b)

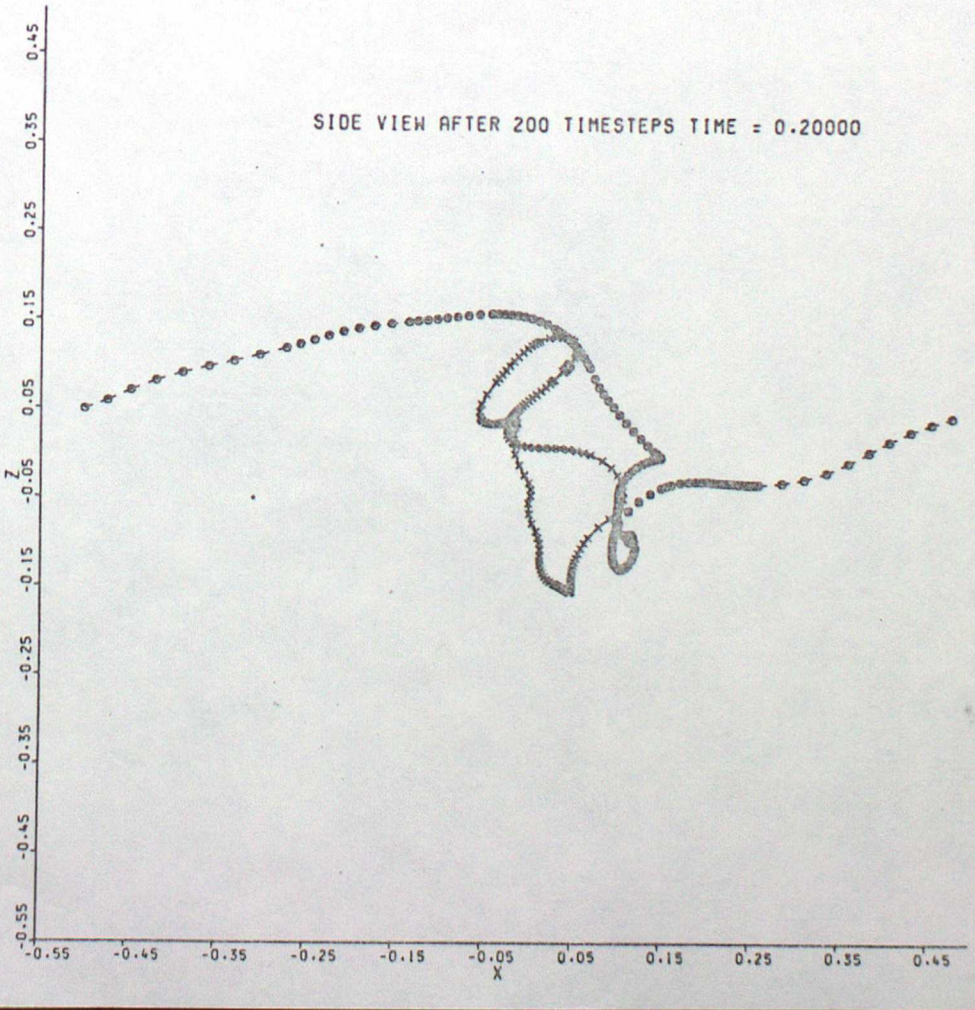

Figure 4.3

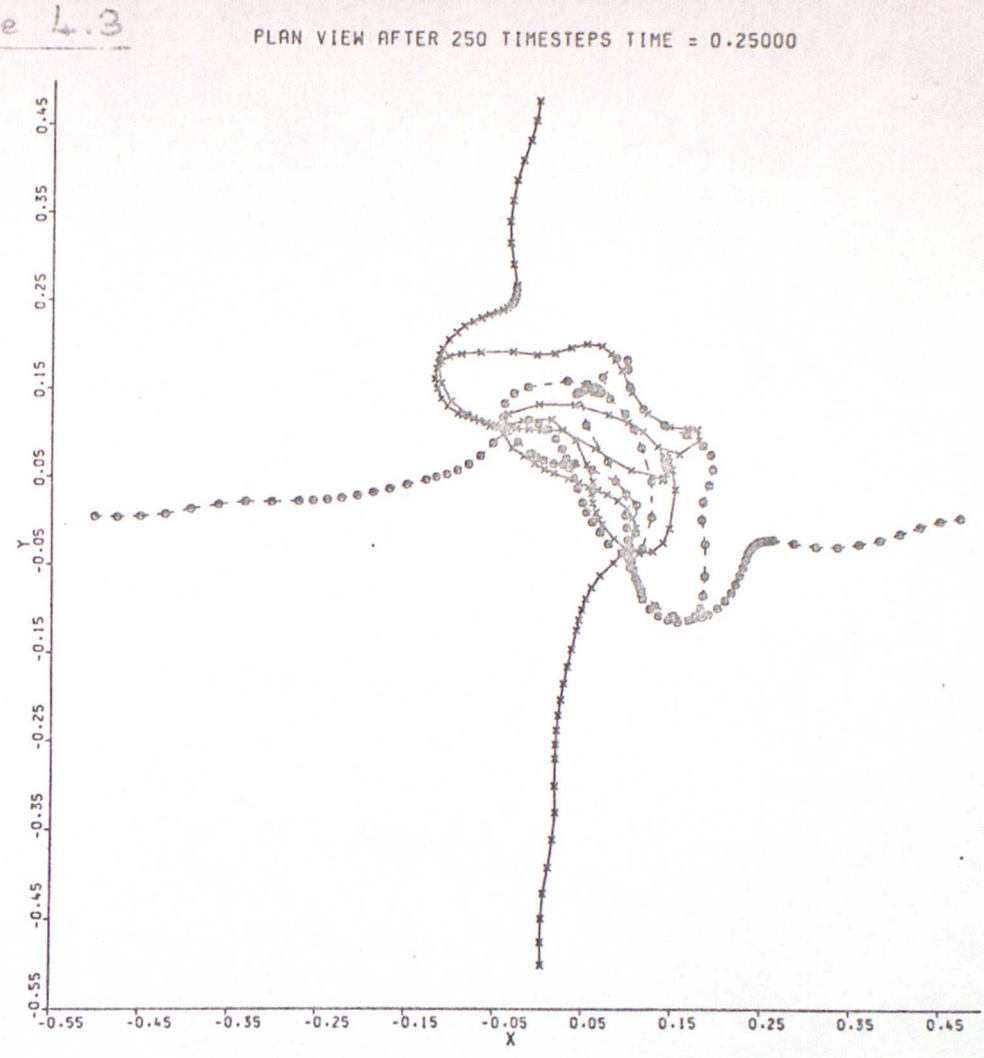

Figure 4.5

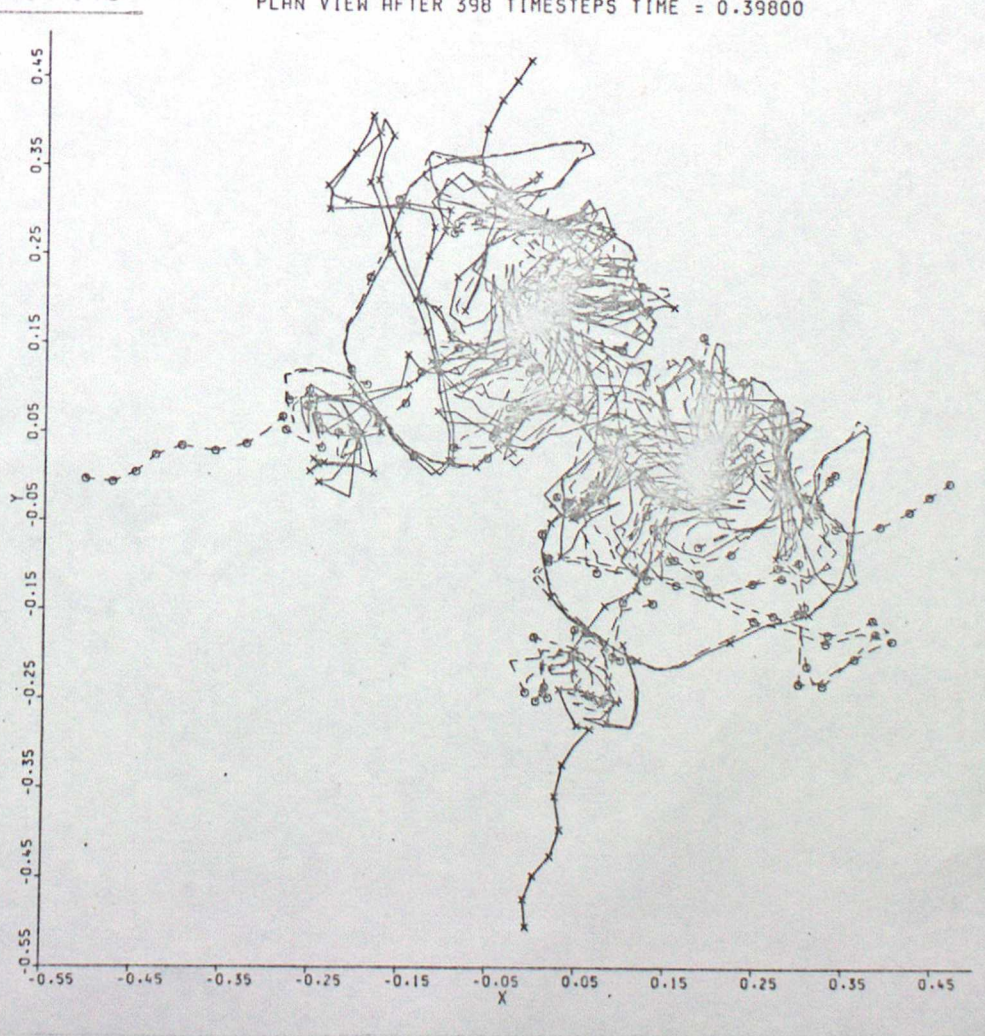

Figure 4.4a)

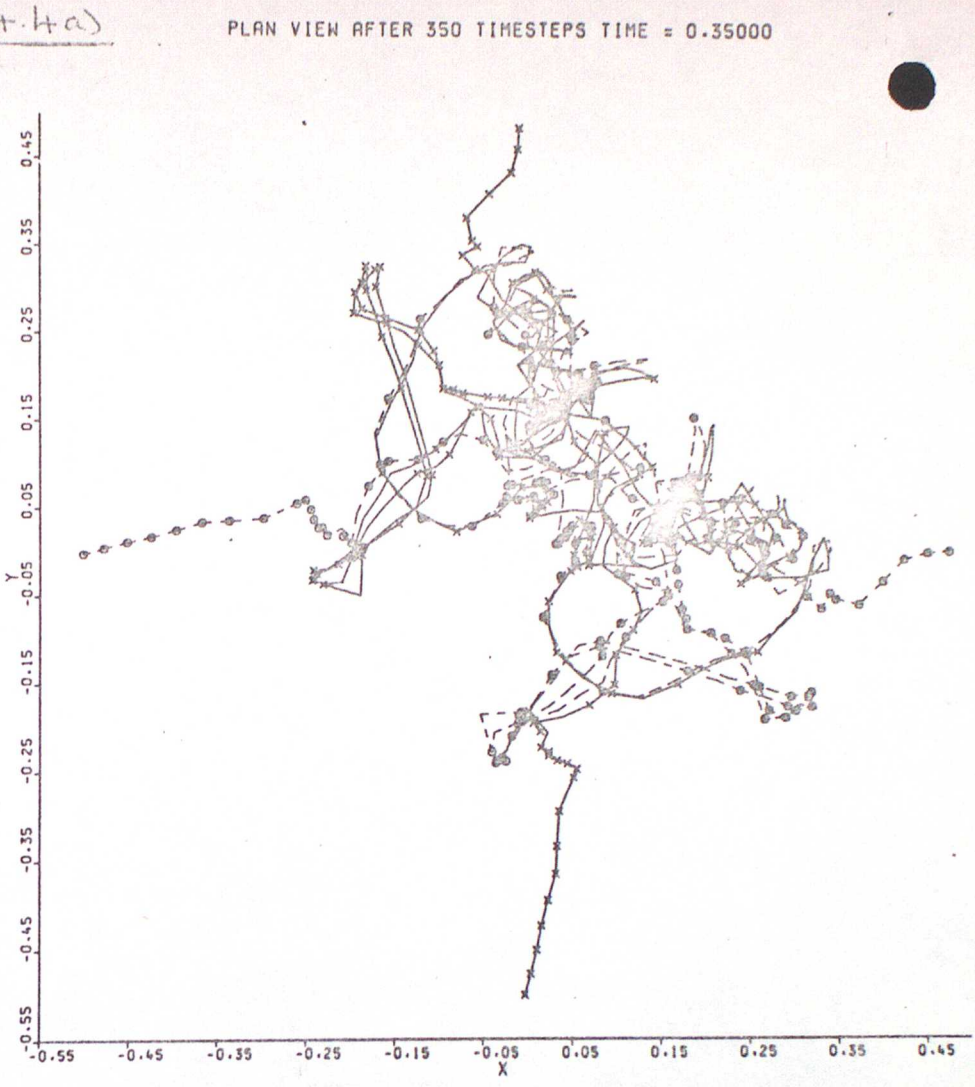

Figure 4.4 b)

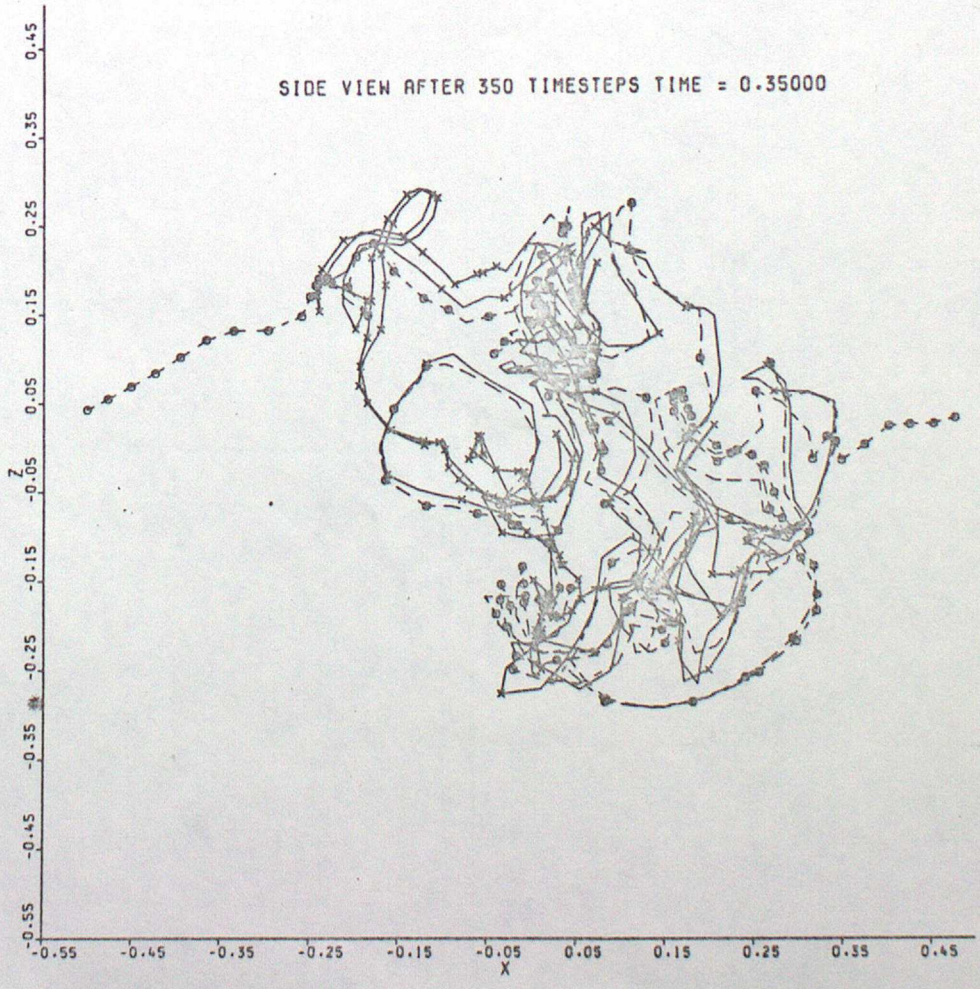

Figure 4.6 3-D Plot of Configuration of the Vortex Filaments

After 398 Timesteps , Time = 0.393

——— 1st filament , originally ∥ to y axis

– – – 2nd filament , originally ∥ to x axis

▷ direction of vorticity

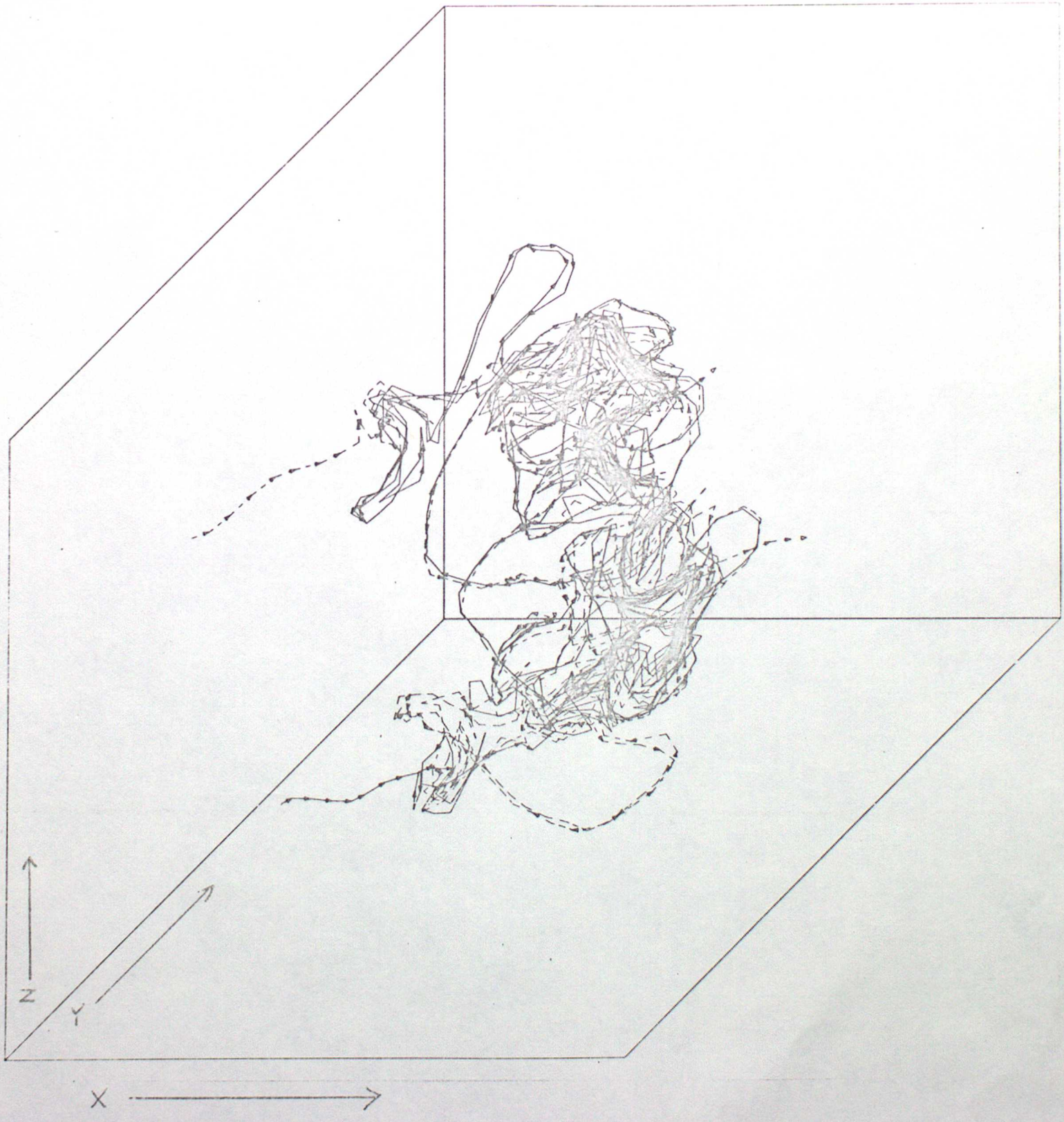

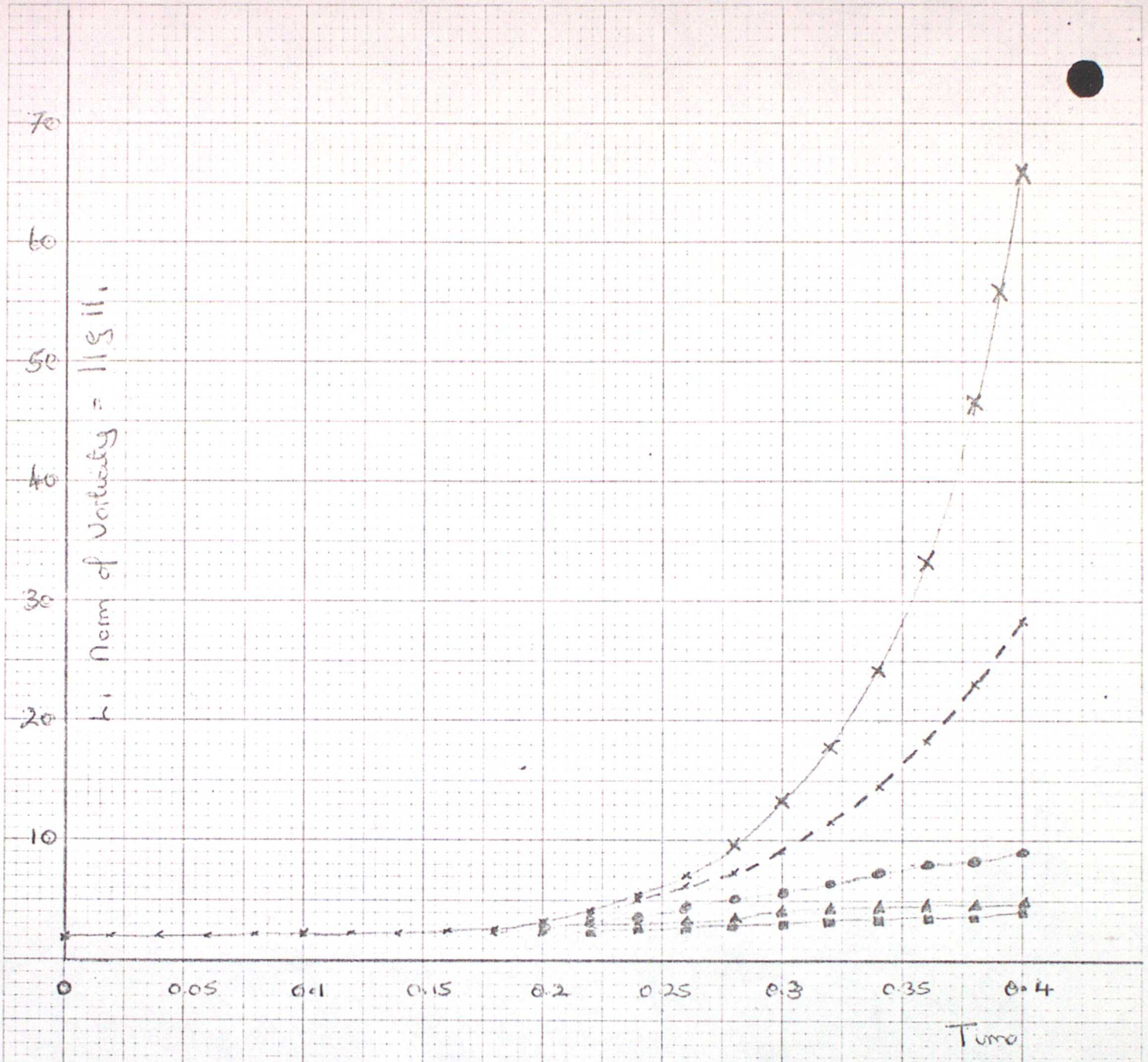

Figure 4.7 Evolution of L_1 Norm of Velocity for Vortex filaments with circulation = 1

For Standard Integration
4th order Runge-Kutta time integration
time step = 0.001
Rmax = 0.495
Rmin = 0.05

Chorin's Method

Beale and Majda's Method
H = 0.00312S
H = 0.0125
H = 0.025
H = 0.05

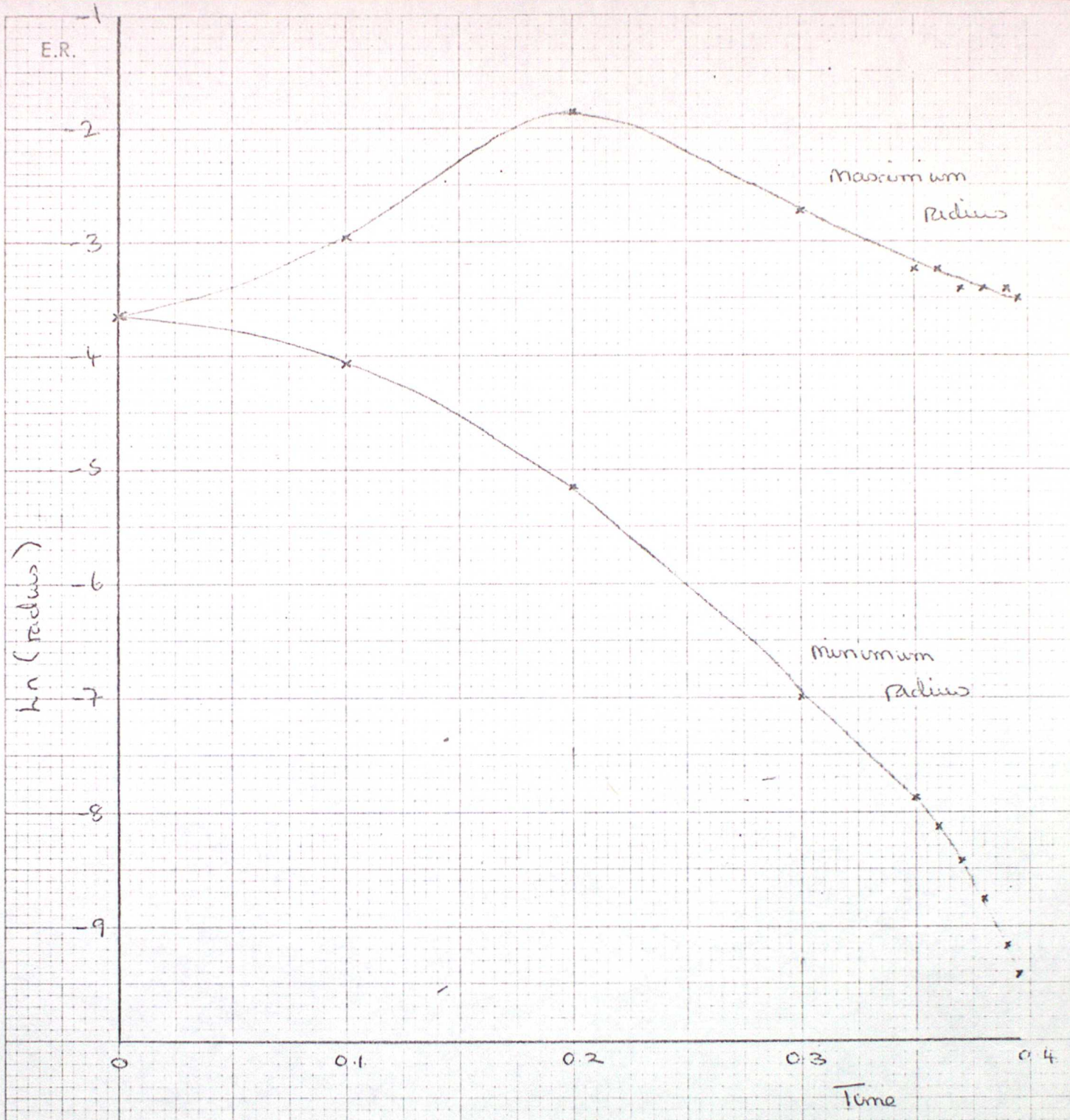

Figure 4.8 Evolution of core radius (stretching)

Time	CHORIN			
	h_2 Norm of Vorticity per filament	Minimum Radius	Maximum Radius	Number of Segments per filament
0	5.1×10^{-2}	0.025	0.025	160
0.1	7.0×10^{-2}	1.7×10^{-2}	0.052	160
0.2	2.6×10^{-3}	5.9×10^{-3}	0.152	160
0.3	2.3×10^{-5}	9.1×10^{-4}	0.065	228
0.35	1.9×10^{-6}	3.8×10^{-4}	0.039	446
0.36	2.9×10^{-6}	2.9×10^{-4}	0.031	508
0.37	4.9×10^{-6}	2.2×10^{-4}	0.033	599
0.38	8.4×10^{-6}	1.6×10^{-4}	0.033	697
0.39	1.5×10^{-7}	1.0×10^{-4}	0.033	843
0.395	2.0×10^{-7}	8.2×10^{-5}	0.030	929
0.398	2.4×10^{-7}	7.1×10^{-5}	0.029	982

Table 4.3 Evolution of h_2 norm of vorticity (enstrophy) and minimum and maximum radii of segments for the standard integration

Figure 4.9

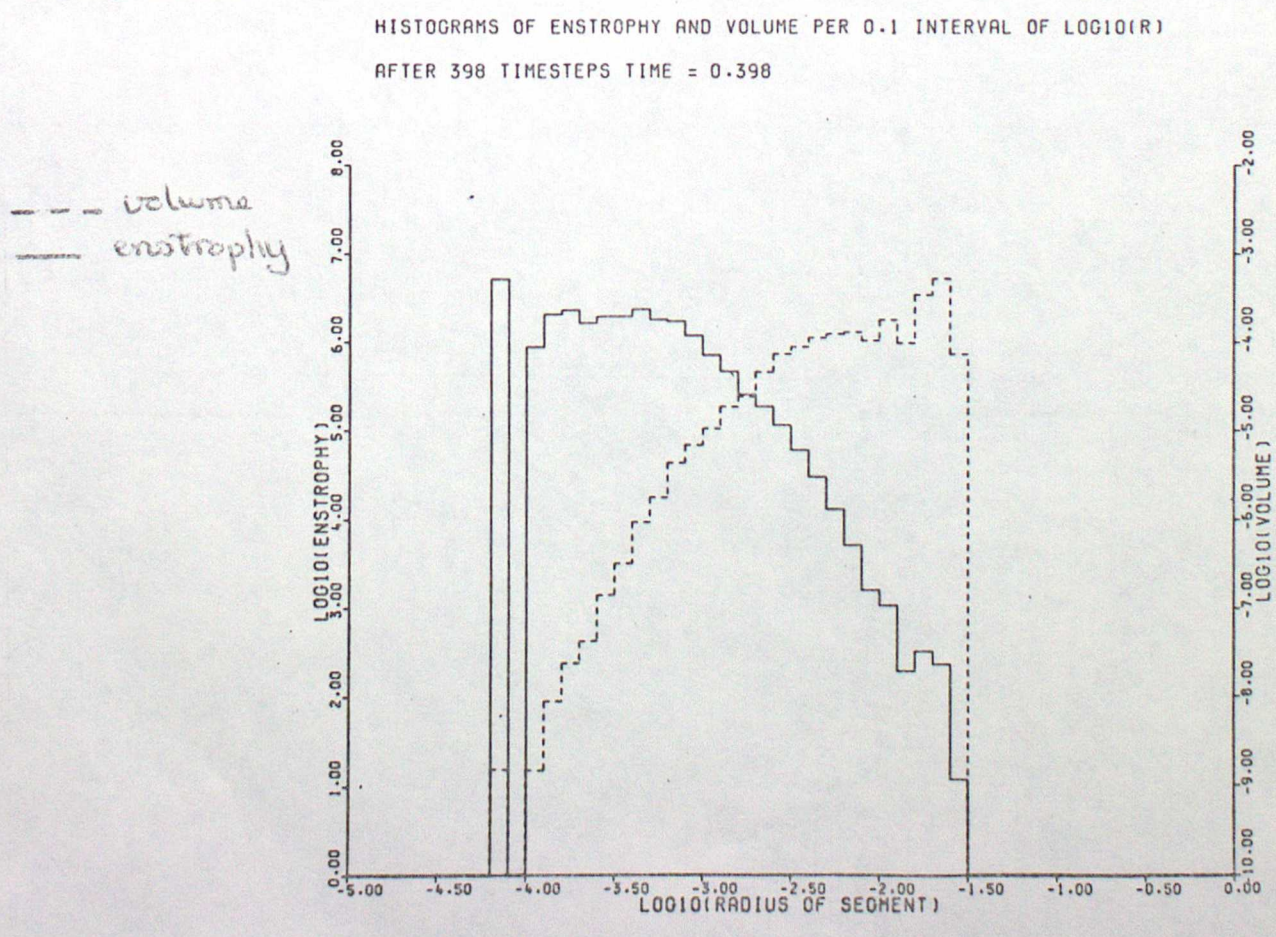

Figure 4.10a)

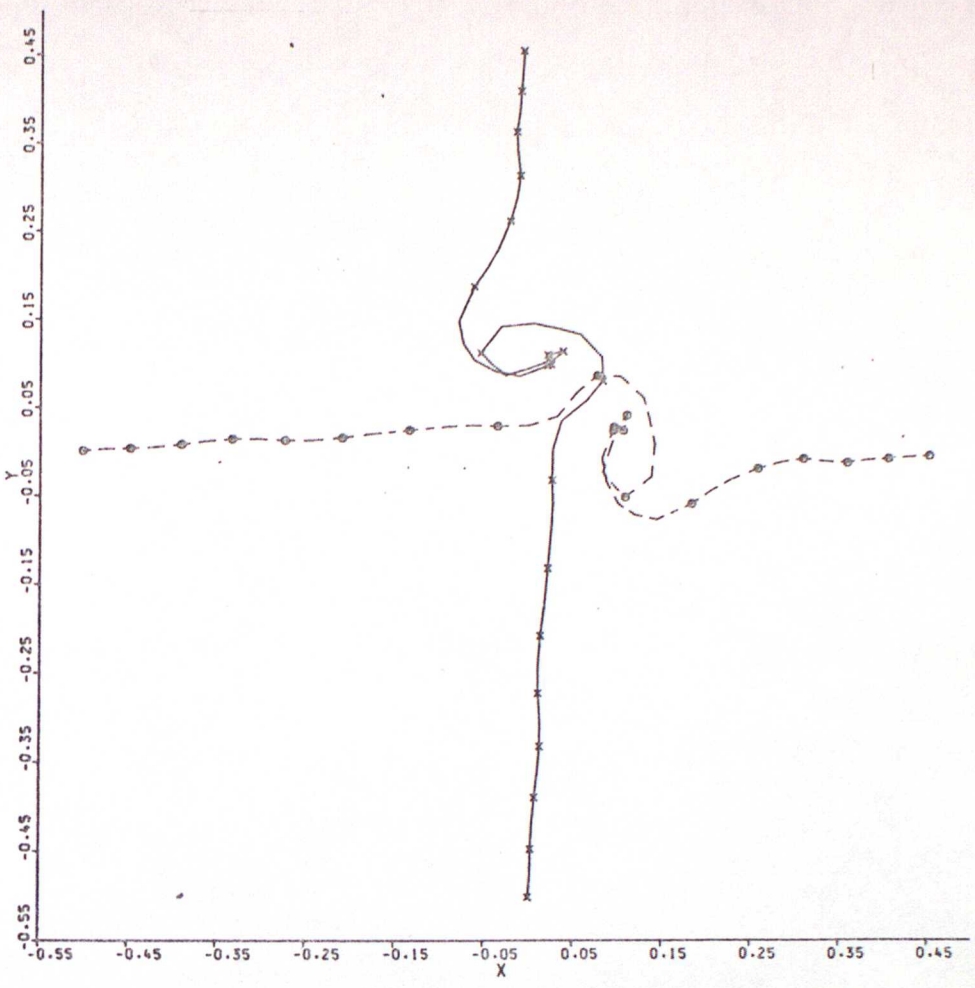

Figure 4.10b)

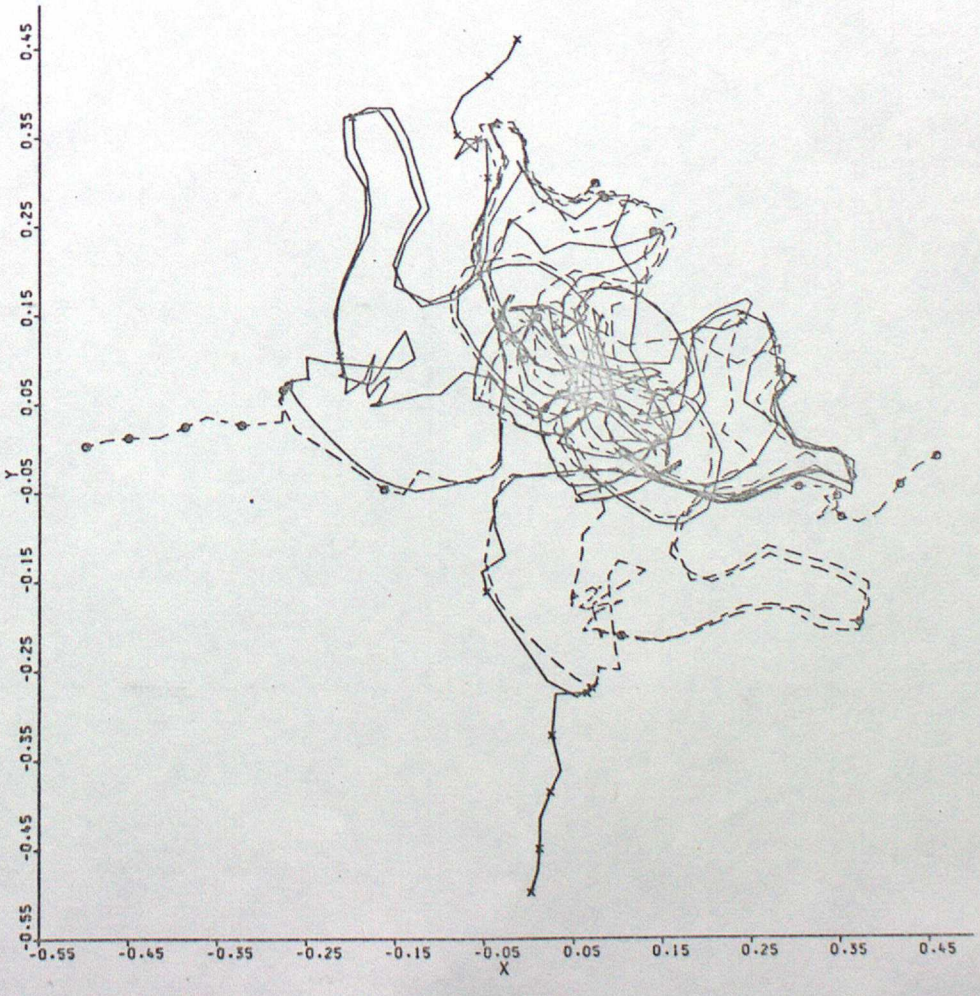

Figure 4.11

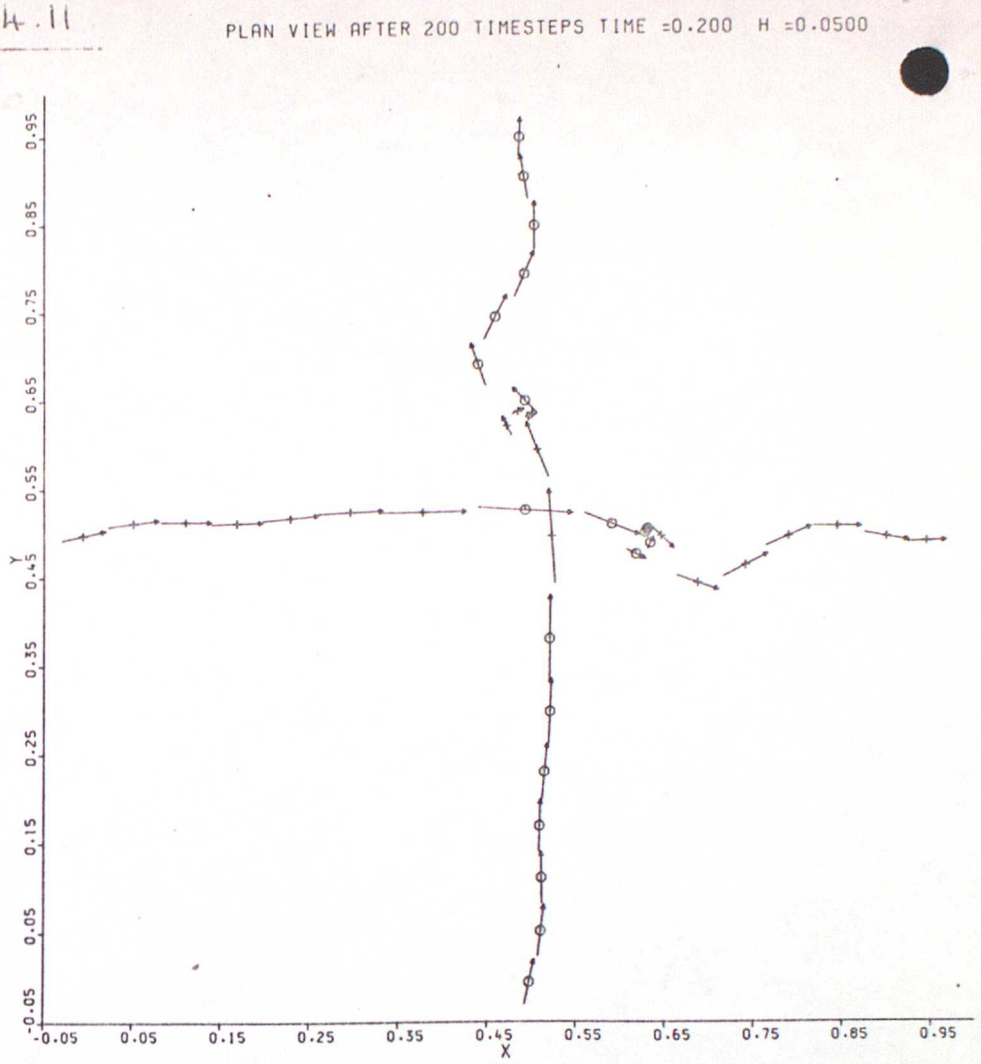

Figure 4.12

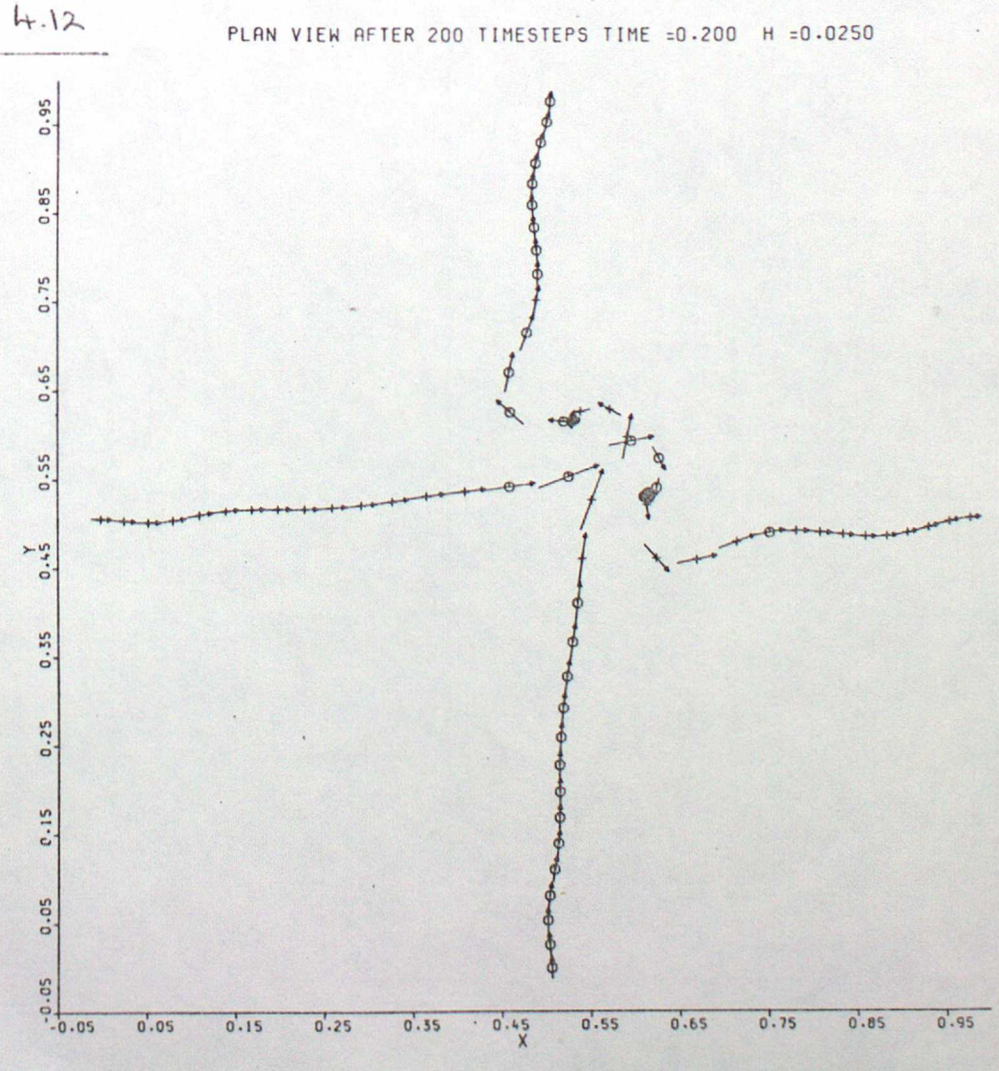

Figure 4.13

PLAN VIEW AFTER 200 TIMESTEPS TIME =0.200 H =0.0125

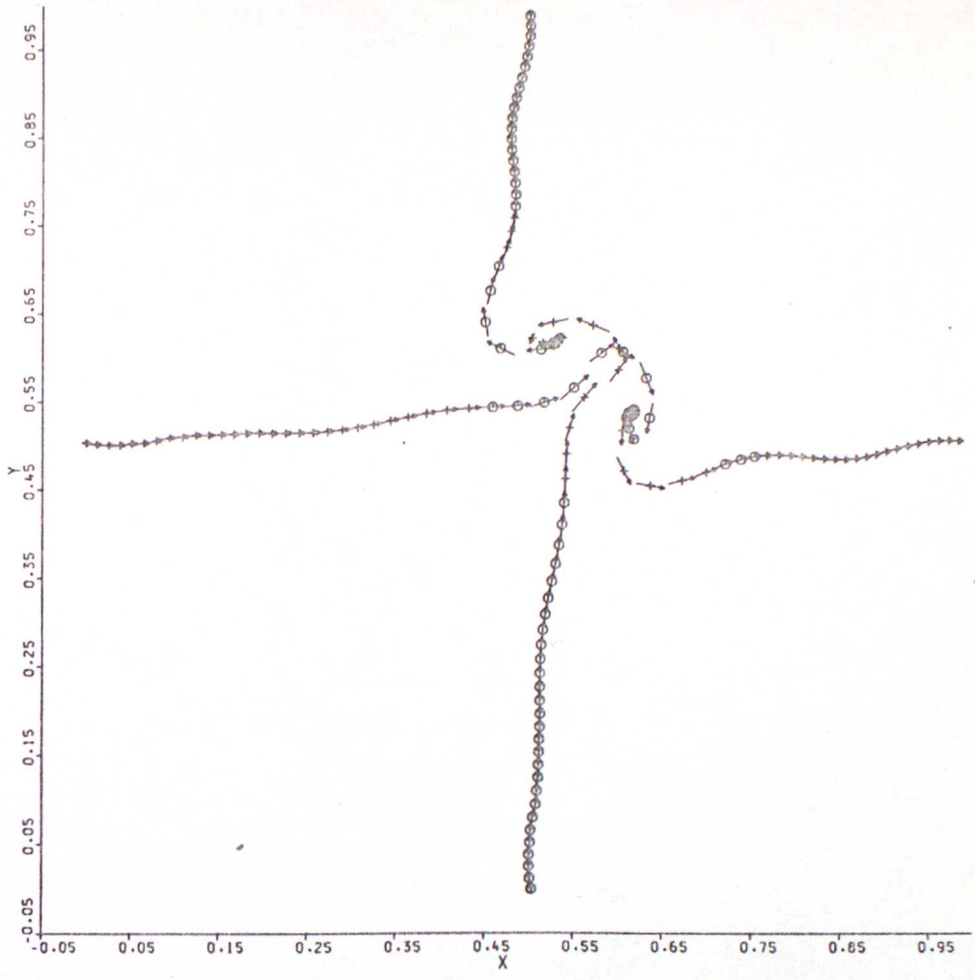

Figure 4.14

PLAN VIEW AFTER 200 TIMESTEPS TIME =0.200 H =0.003125

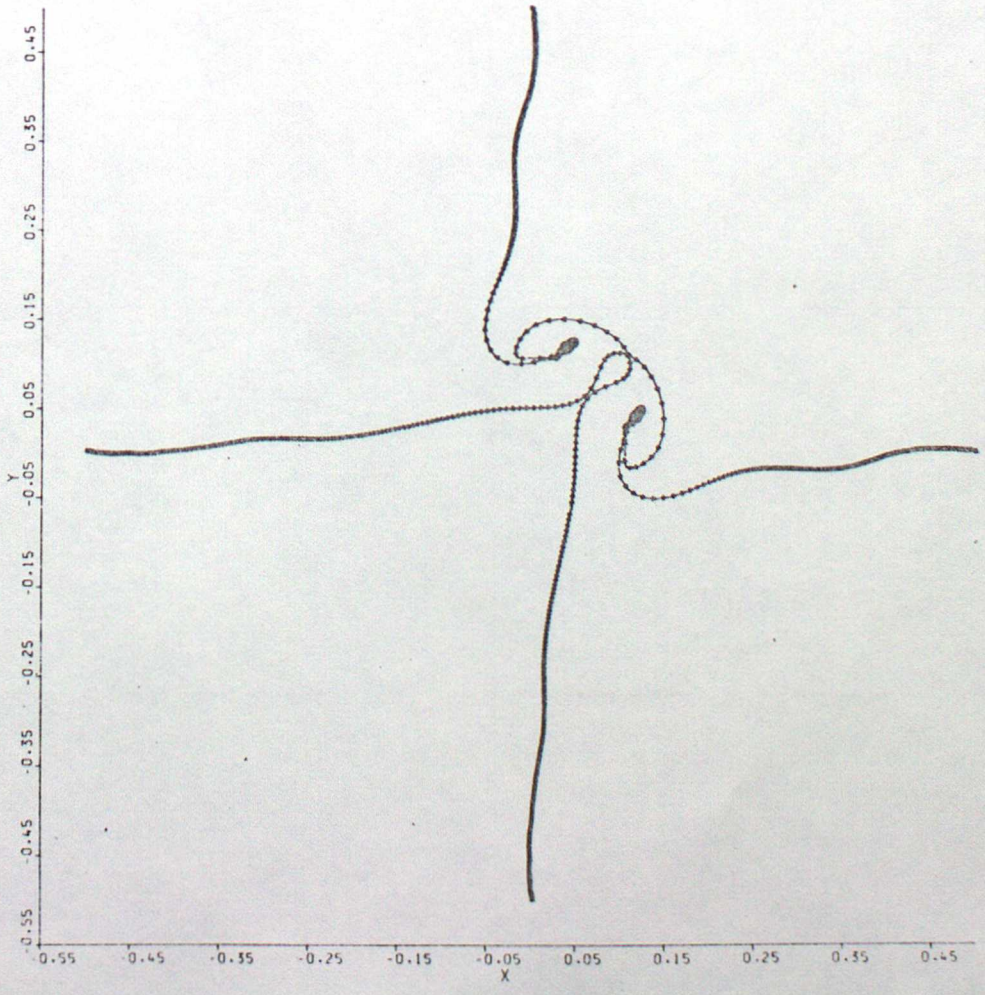

Figure 4.15

PLAN VIEW AFTER 250 TIMESTEPS TIME =0.250 H =0.003125

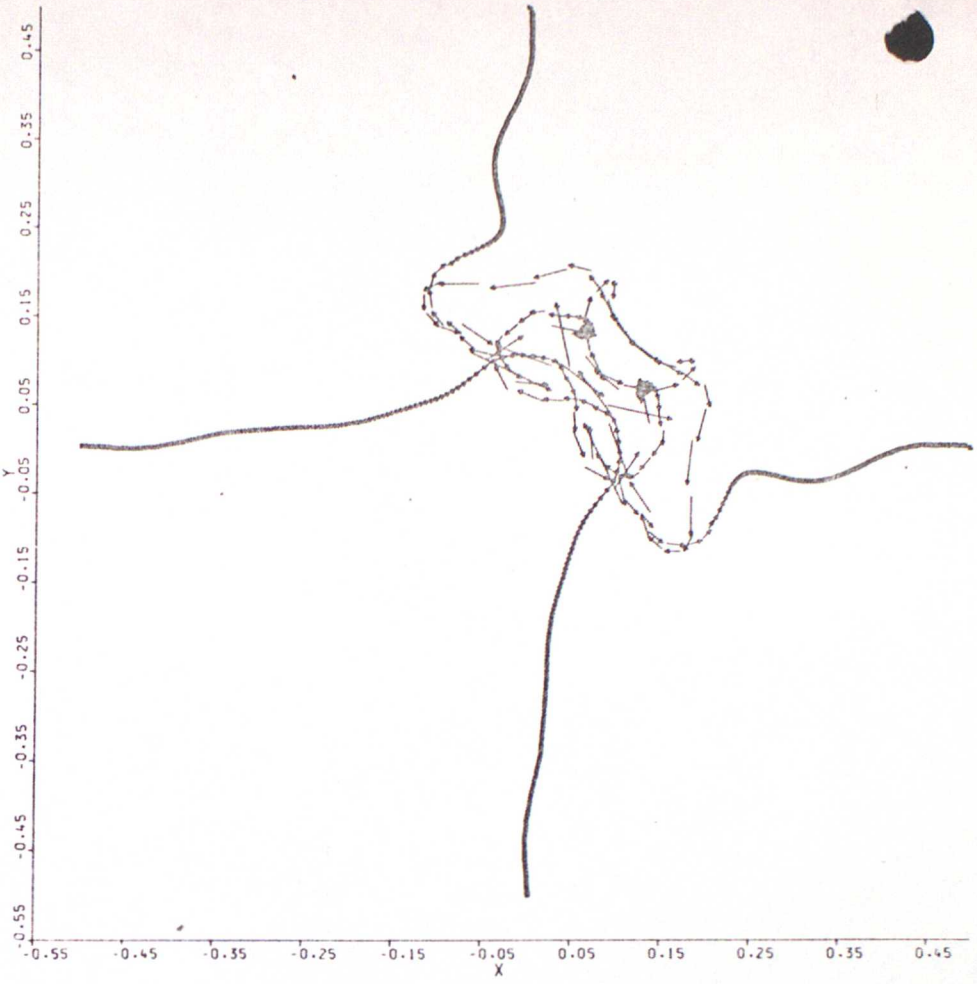

Figure 4.16

PLAN VIEW AFTER 350 TIMESTEPS TIME =0.350 H =0.003125

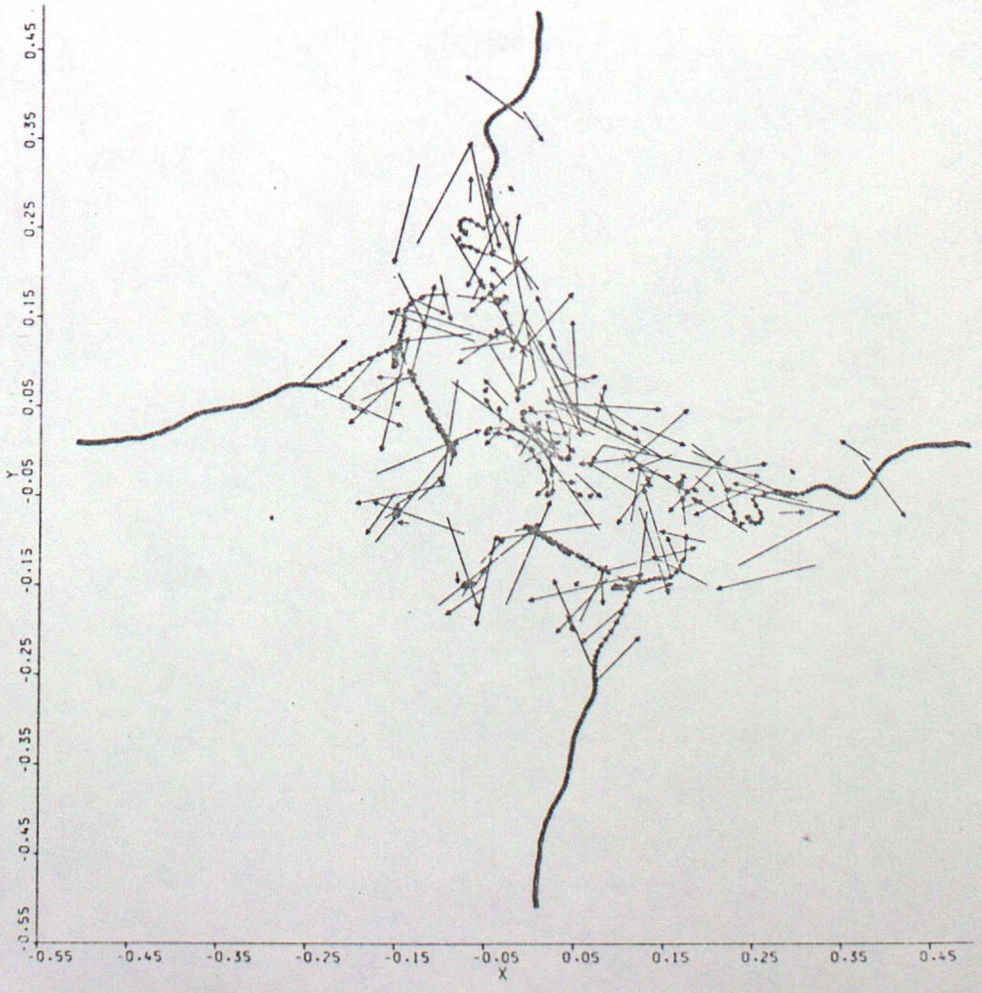

Figure 4.17

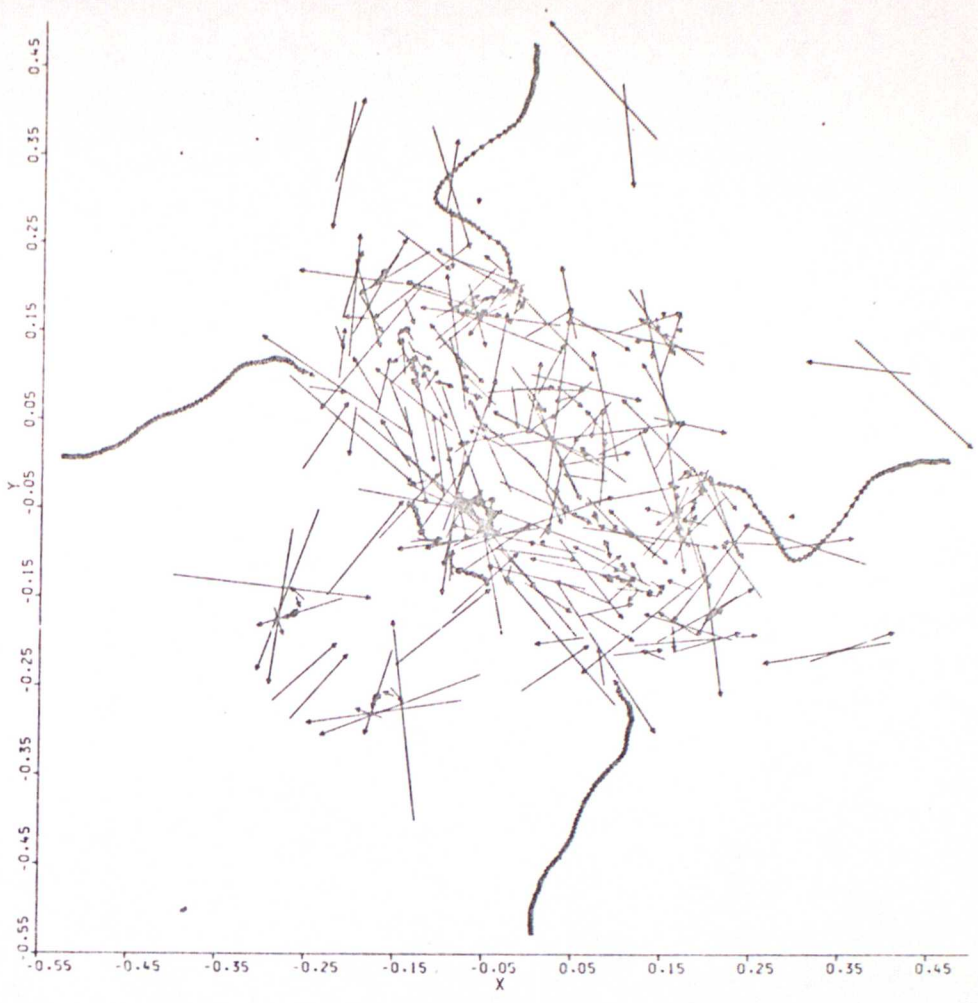
PLAN VIEW AFTER 400 TIMESTEPS TIME =0.400 H =0.003125
0.45
0.35
0.25
0.15
0.05
-0.05
-0.15
-0.25
-0.35
-0.45
-0.55
Y
-0.55
-0.45
-0.35
-0.25
-0.15
-0.05
0.05
0.15
0.25
0.35
0.45
X